Eur. J. Mineral., 37, 841–869, 2025 https://doi.org/10.5194/ejm-37-841-2025 © Author(s) 2025. This work is distributed under the Creative Commons Attribution 4.0 License.





Formation of the Ertelien and Langedalen magmatic Ni–Cu sulfide deposits in Norway: investigating the evolution of platinum-group-element-depleted systems at convergent margins

Eduardo Mansur¹, Alf Andre Orvik¹, Iain Henderson¹, Ana Carolina Miranda¹, Trond Slagstad¹, Sarah Dare², Terje Bjerkgård¹, and Jan Sverre Sandstad¹

¹Geological Survey of Norway, P.O. Box 6315 Torgarden, Trondheim, 7491, Norway ²Département de Sciences Appliquées, Université du Québec à Chicoutimi, QC G7H 2B1, Chicoutimi, Canada

Correspondence: Eduardo Mansur (eduardo.mansur@ngu.no)

Received: 26 May 2025 - Revised: 8 August 2025 - Accepted: 15 September 2025 - Published: 4 November 2025

Abstract. The Ertelien and Langedalen magmatic Ni-Cu sulfide deposits are hosted within mafic intrusions of the Kongsberg Lithotectonic Unit in the southwestern Fennoscandian Shield, formed in a convergent-margin tectonic setting. The Ertelien deposit occurs within a gabbronorite intrusion of approximately 600 × 500 m, with the main sulfide mineralization being located at the contact with the surrounding gneiss. In contrast, the Langedalen deposit consists of 1-2 m massive sulfide lenses hosted in 10-50 m gabbronorite lenses that are extensively deformed within shear zones. Sulfide mineralization in Ertelien ranges from disseminated to nettextured and massive ores, whereas Langedalen ranges primarily comprise massive sulfide lenses. A distinctive feature of Langedalen ranges is the local presence of an Au-rich quartz vein adjacent to the sulfide lenses. In both deposits, pyrrhotite is the dominant sulfide mineral, followed by pentlandite and minor chalcopyrite. Secondary pyrite is present, particularly in altered zones. This study provides a comprehensive characterization of the Ertelien and Langedalen deposits and constrains their genesis within a convergent-margin context. We analysed S, platinum group elements (PGEs), TABS+ (Te, As, Bi, Sb, Se), and other chalcophile elements in whole rocks and sulfide minerals across different ore textures, as well as U-Pb and Hf isotopes in zircon. Wholerock geochemistry reveals a positive correlation between S and Ni, Cu, and Co, with sulfide tenors of ca. 2.2 wt % Ni, 1.5 wt % Cu, and 1200 ppm Co. Sulfides from both deposits are notably depleted in PGEs, consistently with derivation from a PGE-depleted parental magma compositionally similar to cogenetic dykes. This depletion may result from an event of prior sulfide segregation. However, we suggest that an alternative explanation is that the parental magmas were derived from a hydrous metasomatised pyroxenitic mantle source. In addition, a zircon U-Pb crystallization age of $1559 \pm 7 \, \text{Ma}$ and $\varepsilon \text{Hf}(i)$ values of +3 to +5 for the Ertelien intrusion support formation during a prolonged subduction-related magmatic episode involving oceanic crust recycling. Despite post-magmatic alteration and secondary pyrite formation, sulfide minerals largely preserve their primary magmatic signatures, comparably to other Ni-Cu magmatic systems globally. However, parts of the Langedalen sulfides exhibit hydrothermal overprint, reflected in elevated concentrations of mobile elements (Te, As, Bi, Sb), likely linked to the formation of the Au-rich quartz vein.

1 Introduction

Magmatic sulfide deposits have been extensively studied over the last few decades (Barnes and Lightfoot, 2005; Naldrett, 2011), and the combination of the knowledge derived from these studies allows for a holistic view of the magmatic systems in which they form (Barnes et al., 2016). A common feature of most conceptual models for the formation of magmatic sulfide deposits is the generation of parental magmas through plume-driven melting of dry peridotite sources (Begg et al., 2010; Maier and Groves, 2011; Naldrett, 2011). Still, some deposits are likely not to be explainable by large degrees of partial melting, supporting the fact that some important variations in conceptual models may exist. For instance, recent studies favour the involvement of pyroxenitic mantle sources in the generation of parental magmas for some non-komatiitic Ni-Cu sulfide deposits (Lu et al., 2019). Indeed, magmas produced from a pyroxenite mantle source are argued to be enriched in Ni (Sobolev et al., 2005) and could be regarded as fertile for the formation of Ni-Cu sulfide deposits (Blanks et al., 2025; Ezad et al., 2024).

An interesting consequence of changes in conceptual models for the formation of magmatic sulfide deposits is the implications of their formation within geodynamic settings that were not previously regarded as fertile. For instance, convergent and collisional settings were not traditionally considered to be prospective for magmatic sulfide deposits compared to other settings such as craton margins where lithospheric thinning and adiabatic mantle melting would lead to high degrees of partial melting (Begg et al., 2010; Maier and Groves, 2011; Griffin et al., 2013). However, convergent settings may allow for oceanic crust recycling and the development of pyroxenitic mantle domains (Sobolev et al., 2005; Ezad et al., 2024). The implications of a metasomatised mantle source are highlighted by assessing the mineralogical distribution of Ni in metasomatised mantle xenoliths, in which Ni is partially hosted within hydrous phases such as phlogopite and amphibole (Blanks et al., 2025). Therefore, melting of such metasomatised mantle domains would lead to the formation Ni-rich magmas at relatively low-temperature ranges (ca. 300–350 °C lower than dry peridotites, around 1090 °C) (Ezad et al., 2024; Foley et al., 2022), opening a window of opportunity for reviewing the prospectivity of magmatic sulfide deposits in convergent settings.

An important step for reviewing the potential for the formation of magmatic Ni–Cu deposits in convergent and collisional settings is systematically studying and understanding the formation of known occurrences. For instance, previous investigations have highlighted that several magmatic sulfide occurrences in arc-related settings are depleted in platinum group elements (PGEs) (Mansur et al., 2023b, c; Jesus et al., 2020; Lu et al., 2019). Although such a geochemical feature may be explained by an S saturation event prior to magma emplacement at shallower crustal levels (Lightfoot et al., 2012), this can also be reconciled with magmas derived from

a metasomatised mantle source (Blanks et al., 2025; Ezad et al., 2024). The reasoning is that, although, in metasomatised mantle domains, Ni could still be sourced from hydrous silicates, PGE-bearing sulfides may have already been extracted upon oceanic crust recycling. This would provide an explanation for the systematic occurrence of PGE-depleted magmatic sulfide deposits in arc-related geodynamic settings (Lu et al., 2019).

Several PGE-depleted magmatic Ni-Cu sulfide occurrences have been described in the southern parts of Norway (Barnes et al., 1988). These systems form as part of relatively geographically extensive mafic magmatism, and recent contributions support their development within an arcrelated tectonic setting (Orvik et al., 2025). However, most of these occurrences still lack a systematic characterization and understanding of the processes involved in their petrogenesis. In this context, two of these occurrences, Ertelien and Langedalen Ni-Cu deposits, were previously identified (Barnes et al., 1988; Niarezka, 2023), but their formation was not assessed in detail. In this contribution, we combine field and petrographic observations, whole-rock and sulfide mineral compositions, and U-Pb and Hf isotopic analyses in zircon to investigate the formation of the Ertelien and Langedalen deposits. The results are discussed in light of the development of PGE-depleted systems within a convergent tectonic setting as supported by previous contributions, and we explore the possibility that parental magmas for these deposits formed from a hydrous metasomatic pyroxenite source.

2 Regional setting

The SW portion of Fennoscandia during the period between ca. 1.9 and 1.4 Ga can be regarded to be characterized by oceanward growth along an overall retreating continental margin (Åhäll and Connelly, 2008; Andersen et al., 2004; Bingen et al., 2005; Roberts and Slagstad, 2015; Roberts et al., 2013). During this period, different accretionary orogenies are identified, namely the Svecofennian (1.91–1.75 Ga), Transscandinavian Igneous Belt (TIB; 1.86-1.66 Ga), Gothian (1.66–1.52 Ga), Telemarkian (1.52–1.48 Ga), and Hallandian (1.47-1.38 Ga) (Roberts and Slagstad, 2015; Bingen et al., 2021; Stephens and Wahlgren, 2020; Ulmius et al., 2015). Overall, these orogenies mark the evolution of geological provinces that are divided into five main lithotectonic units (LTUs), from east to west: the Eastern Segment, Idefjorden, Kongsberg, Bamble, and Telemark (Fig. 1a) (Bingen et al., 2021; Slagstad et al., 2020; Slagstad et al., 2024; Scheiber et al., 2015; Scheiber et al., 2023).

The Kongsberg LTU, which hosts the mineral occurrences investigated in this contribution, encompasses the Kongsberg Complex, divided into the Eastern Segment and the Western Segment by the Modum Complex (Fig. 1b). The Eastern and Western Kongsberg complexes comprise intercalations of

metavolcanic and metasedimentary sequences, whereas orthogneisses yield magmatic crystallization ages ranging from 1.57 to 1.48 Ga (Scheiber et al., 2023; Andersen et al., 2004; Bingen and Viola, 2018). The Modum Complex is dominated by a quartz-rich metasedimentary succession deposited after the crystallization of the Kongsberg Complex (Bingen et al., 2001; Bingen and Viola, 2018; Scheiber et al., 2023). The Kongsberg LTU was affected by early-Sveconorwegian metamorphism, which progressed from amphibolite facies in the West Kongsberg Complex to upper amphibolite facies within the Modum Complex and to granulite-facies metamorphism in the East Kongsberg Complex (Scheiber et al., 2023). The timing of metamorphism has been constrained to ca. 1145-1080 Ma, which encompasses the development of high-grade and further retrograde assemblages (Munz et al., 1994; Bingen and Viola, 2018; Bingen et al., 2021; Scheiber et al., 2023).

Several mafic (and, rarely, ultramafic) intrusions occur within the Kongsberg LTU (Bingen and Viola, 2018; Viola et al., 2016), which are commonly metamorphosed and transformed into garnet amphibolite. In a recent contribution, Orvik et al. (2025) integrated U–Pb and Lu–Hf isotopic data in zircon from a wide range of mafic and felsic intrusive bodies from the different portions of the Kongsberg LTU. The authors offer support for those intrusions from the East Kongsberg Complex aligning with Gothian magmatism (ca. 1610 to 1524 Ma), whereas those from the West Kongsberg Complex record younger, more juvenile magmatism (1529 to 1153 Ma), consistently with their formation within an arc-related tectonic setting. In contrast, the Modum Complex represents an extensional basin development and juvenile mafic magmatism between ca. 1305 and 1185 Ma.

Magmatic sulfide occurrences in the Kongsberg lithotectonic unit

Several magmatic Ni-Cu sulfide occurrences were identified within the Kongsberg LTU and grouped as part of the Ringerike Ni-Cu metallogenic province (Sandstad et al., 2012). This province encompasses the Veme Complex (metasedimentary successions correlated with the Stora Le-Marstrand Complex east of the Oslo rift; Åhäll and Connelly, 2008), the East Kongsberg Complex, and parts of the West Kongsberg Complex (Fig. 2). The province includes the Ertelien deposit, which was a significant historic producer in the area (Boyd and Nixon, 1985), and the Langedalen deposit, which was a smaller producer, and both are the subject of this contribution. Additionally, 11 smaller mines and numerous other nickel occurrences, with a total of 23 registered occurrences in the NGU national database, were identified (Sandstad et al., 2012). Orvik et al. (2025) reported zircon U-Pb magmatic crystallization ages from the Langedalen deposit ranging from 1546 ± 2 to 1524 ± 11 Ma, along with a mafic dyke interpreted as being correlated with the Ertelien deposit at 1584 ± 19 Ma. The authors argue that the main Ni–Cu deposits from the Ringerike Ni–Cu metallogenic province predominantly correlate with Gothian magmatism. In contrast, smaller deposits found within West Kongsberg (Fig. 1b), such as Grågalten (1164 \pm 13 Ma), are linked to later magmatic events.

Previous work on the Ertelien deposit indicates that it is located at the margins of a small gabbronorite intrusion (Niarezka, 2023). The mineralization ranges from low-grade disseminations to high-grade massive sulfides from the centre towards the base of the intrusion, respectively. The ore mineral assemblage is dominated by pyrrhotite, followed by pentlandite, pyrite, and chalcopyrite, with both Ni-rich and Cu-rich ores present. Historical production estimates for Ertelien vary from a minimum of 280 kt at 1 % Ni and 0.8 % Cu to 400 kt at 1.04 % Ni, 0.69 % Cu, and 0.17 % Co (Sandstad et al., 2012). Based on the metal ratios and PGEdepleted nature of the sulfides, Barnes et al. (1988) proposed that the deposit originated from a primitive magma, from which sulfides were extracted prior to the intrusion emplacement. An investigation by Niarezka (2023), focusing on petrographic description and whole-rock and mineral chemistry, suggested that S saturation was triggered by the assimilation of S-bearing country rocks. Still, the author notes that the evolution of the deposit likely involved different stages, which were not investigated in detail, and points to the need for future work to comprehensively understand its petrogenesis. Current exploration work and drilling at the Ertelien deposit have resulted in a mineral resource estimate of approximately 23 Mt at 0.21 % Ni, 0.16 % Cu, and 0.014 % Co (Kuniko, 2024). Although these grades are significantly lower than historical production, the resource estimate includes higher-grade zones, totalling ca. 4.6 Mt at 0.44 % Ni, 0.34 % Cu, and 0.030 % Co.

The Langedalen mine was active in the late 1800s and produced approximately 10 kt of ore, with nickel grades ranging from 2.5 % to 3.5 % (Mathiesen, 1977). Although it is much smaller relative to the Ertelien deposit, Langedalen represent a different style of mineralization, where the sulfide ore is hosted within very deformed mafic lenses trending towards approximately 320°, with a near-vertical plunge (Reddick and Armstrong, 2009). Therefore, the rationale for studying and comparing Ertelien and Langedalen deposits is to investigate Ni–Cu occurrences with variable degrees of deformation and alteration within the same province. No systematic study of the mineralization has been carried out before. A peculiar feature of the Langedalen deposit is the local occurrence of an Au-rich quartz vein yielding ca. 150 ppm Au over 0.4 m (Bjerkgård et al., 2020).

3 Materials and methods

We have systematically sampled two drill cores from the Ertelien deposit (ER-2006-05 and ER2006-06B) and one drill core from the Langedalen deposit (LN07-09). The sam-

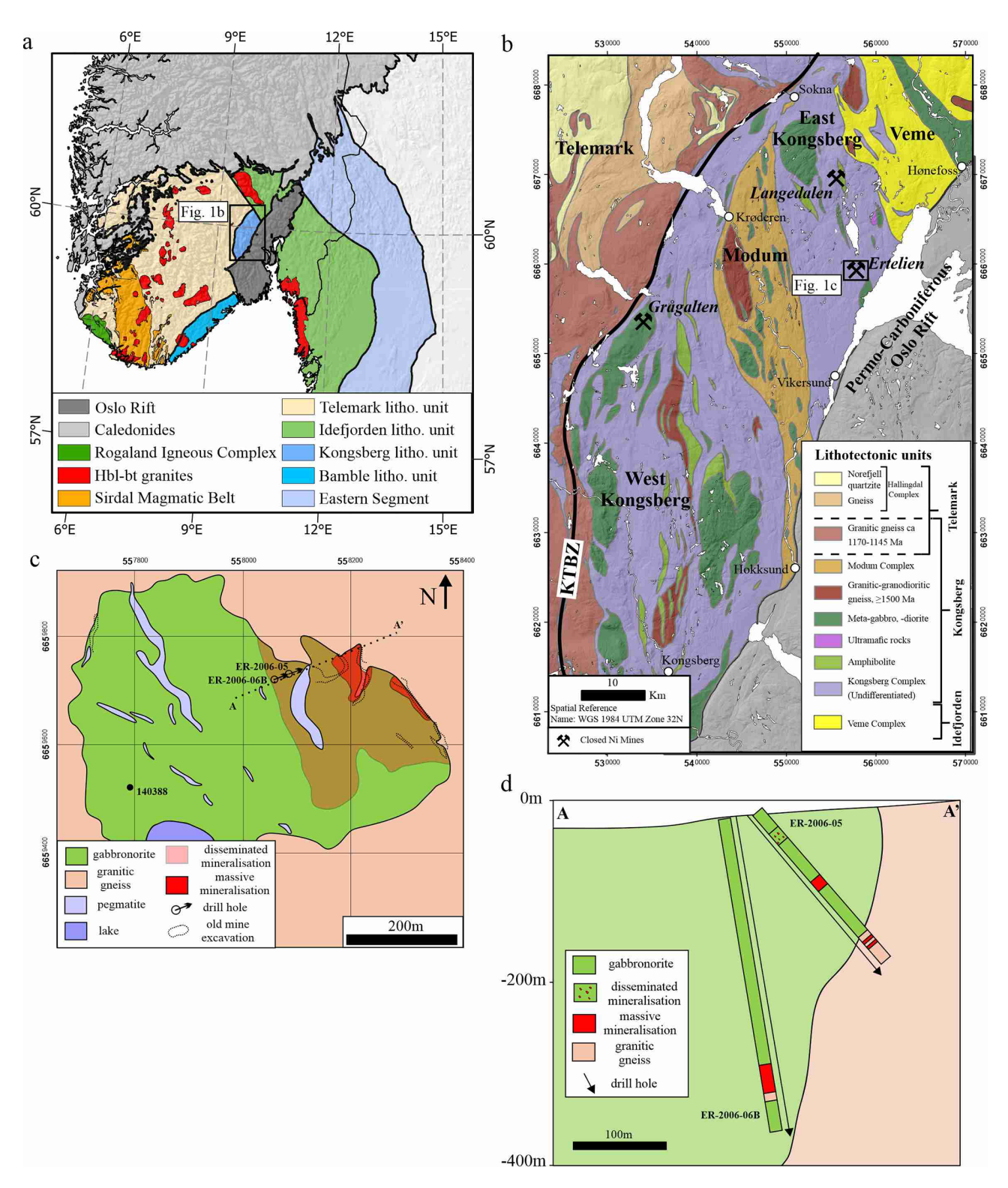


Figure 1. (a) Sketched map of southwestern Fennoscandia, showing the major geological domains. (b) Bedrock map of the Kongsberg lithotectonic unit and adjacent units. Modified from Scheiber et al. (2015). (c) Sketch map of the Ertelien intrusion and the associated Ni–Cu sulfide mineralization. (d) Schematic vertical profile across the northwestern part of the Ertelien intrusion, displaying the projection of the two investigated drill cores in this study.

ples were selected with the support of lithogeochemical data for whole-rock S, Ni, and Cu and cover the main ore textures found within the deposits. Samples comprising massive, nettextured, and disseminated sulfides were included. In addition, one gabbronorite surface sample from the Ertelien deposit (sample no. 140388) was collected for zircon U–Pb and Hf isotope analyses, and one sample from a mafic dyke (sample no. 124723) in the vicinity of the Ertelien intrusion was collected as a potential analogue for parental-melt composition (further discussed in the text). The locations of each drill core and each of the surface samples are given in Table S1 in the Supplement.

The exploration geochemical datasets from the studied cores of both the Ertelien and Langedalen deposits were compiled and are reported in Table S2. The sampling interval of the cores for these analyses varies from 0.2 to 2.6 m, with samples covering smaller intervals in mineralized portions and larger intervals within the host rock parts. Sample preparation and lithogeochemical analyses were performed at ALS Chemex. Analytical procedures include whole-rock four-acid digestion with an inductively coupled plasma mass spectrometry (ICP-MS) finish (ALS code: ME-MS61) and Pt, Pd, and Au following the method of PGM-ICP23. Because of the potential limitations of the dataset due to the eventual mixture of different lithologies and different sample sizes, we have mainly limited the use of these results to visualize the main lithogeochemical variations through the cores.

Platinum group elements (PGEs: Os, Ir, Ru, Rh, Pd, and Pt) and Au from 18 samples from the Ertelien deposit, 6 samples from the Langedalen deposit, and 1 sample from a mafic dyke close to the Ertelien deposit (sample no. 124723) were analysed at LabMaTer (Université du Québec à Chicoutimi – UQAC). The PGEs were preconcentrated by Ni sulfide fire assay and co-precipitated with Te and analysed using the solution of ICP-MS following the method described by Savard et al. (2010). International reference materials (OKUM and GeoPT-18/KPT-1 from IAGEO; LK-NIP-1 from Geo Labs – OGS) were analysed with the samples to monitor data quality. The results obtained for the reference materials are consistent with the working values (Table S3). The results for PGEs and Au for the analysed samples are reported in Table S4.

The concentrations and distributions of minor and trace elements in the sulfides were determined by laser ablation (LA)-ICP-MS at the Norwegian Laboratory for Mineral and Materials Characterization (MiMaC) at the Geological Survey of Norway (NGU) using a Teledyne-Cetac Analyte Excite Excimer 193 nm laser equipped with a HelEx II two-volume cell coupled with an Agilent 8900 triple quadrupole (QqQ)-ICP-MS. The LA-ICP-MS tuning parameters were a laser frequency of 10 Hz, a dwell time of 10 ms, a rastering speed of 5 to $10\,\mu m\,s^{-1}$, and a fluence of $2.5\,J\,cm^{-2}$. Line scans across the surface of grains were made with beam sizes of 40 to $50\,\mu m$, depending on the grain size. The gas blank was measured for $30\,s$ before switching on the laser for

around 60 s. The ablated material was carried into the ICP-MS by an Ar-He gas mix at a rate of 0.8 to $1 \, \mathrm{L} \, \mathrm{min}^{-1}$ for Ar and 500 mL min⁻¹ for He (an additional $2 \, \mathrm{mL} \, \mathrm{min}^{-1}$ of nitrogen was also added to the mixture).

Data reduction was carried out using the "Trace Elements" data reduction scheme (DRS) in Iolite 4 (Patton et al., 2011). On-peak gas-blank baselines were fit with an "automatic spline" and subtracted from each channel. To account for variations in ablation yield between samples, stoichiometric Fe values were used for internal standardization of each sulfide.

Three reference materials were used for sulfide external calibration: UQAC-FeS5, a synthetic sulfide developed at UQAC, was used to calibrate for PGEs, Au, and S; MASS-1, which is a ZnCuFeS pressed-powder pellet doped with 50 to 70 ppm of most chalcophile elements, supplied by the United States Geological Survey (USGS), was used to calibrate for Co, Cu, Zn, As, Se, Mo, Ag, Cd, Sn, Sb, Te, Tl, Pb, and Bi; and GSE-1g, which is a synthetic glass doped with most elements at 300 to 500 ppm and is supplied by the USGS, was used to calibrate for Ni, In, and Re using preferred values from the GeoReM database (Jochum et al., 2005). MASS-1, UQAC-FeS-4, UQAC-FeS-6, GSE-1g, GSD-1g, PTC-1b, and CCu-1e were used to monitor the results. The results obtained for these reference materials were in agreement with the accepted values and are provided in Table S5. Polyatomic interference of ⁶³Cu⁴⁰Ar on ¹⁰³Rh was corrected using ¹⁰³Rh measured in MASS-1, which contains 13.4% 63 Cu but no 103 Rh; 1% Cu produced ~ 0.1 ppm interference. Thus, the ¹⁰³Rh values in chalcopyrite are not reported as the interference is too large to be corrected. Direct interferences of ¹⁰⁸Cd on ¹⁰⁸Pd and ¹¹⁵Sn on ¹¹⁵In were corrected by monitoring ¹¹¹Cd and ¹¹⁸Sn, respectively. Interference of ⁶⁸Zn⁴⁰Ar on ¹⁰⁸Pd is negligible. Polyatomic interference of ⁶¹Ni⁴⁰Ar on ¹⁰¹Ru was corrected using ¹⁰¹Ru measured in an NiS blank, which does not contain Ru. On the other hand, 1 % Ni produced ~ 0.007 ppm interference and was not a significant part of the Ru signal. The complete datasets for LA-ICP-MS analyses of pyrrhotite, pentlandite, chalcopyrite, and pyrite, as well as their mass balance results, are provided in Tables S6, S7, S8, and S9, respectively.

Zircons were separated from a gabbronorite sample using traditional techniques, including water table, heavy liquids, magnetic separation, and final handpicking, before mounting in 2.54 cm diameter epoxy rounds. After polishing the mounts, cathodoluminescence (CL) images were obtained to document internal structures, such as growth zoning and core—rim relationships. The CL images for each analysed zircon grain and the positions of each spot analysis are shown in the Table S11.

The U-Pb isotope measurements of zircons were determined by LA-multi collector (MC)-ICP-MS at MiMaC/NGU using a Photon Machines Analyte excite 193 nm excimer laser coupled to an Nu Plasma 3 MC-ICP-MS. The tuning parameters were a laser frequency of 6 Hz, a fluence of

 $2 \,\mathrm{J\,cm^{-2}}$, and a spot size 15 µm. The gas blank was measured for 20 s before switching on the laser for 20 s, followed by a 5 s wash-out period. Ablations were carried out in an He atmosphere, and sample aerosol was transported to the ICP-MS by an He carrier gas, with additional Ar added to the He sample mixture bulb before the plasma torch. The masses 202, 204, 206-208, 232, and 238 were measured. Consistent laser parameters were used for all standards and sample measurements in each sequence. The GJ-1 zircon standard (608.5 \pm 1.5 Ma; Jackson et al., 2004), used as a calibration standard, was analysed at the beginning and end of each run and between every 10 analyses. The reference materials 91500 (1065.4 \pm 0.3 Ma; Wiedenbeck et al., 1995), Z- $6412 (1160 \pm 2 \,\mathrm{Ma}; \,\mathrm{unpublished}, \,\mathrm{GSC} \,\mathrm{Ottawa}), \,\mathrm{and} \,\mathrm{Pleso-}$ vice $(337.13 \pm 0.37; \text{ Sláma et al., } 2008)$ and the in-house standards Temora (416.75 \pm 0.24; Black et al., 2003) and Karasjok (2620 ± 11 Ma; unpublished, NGU) were used to check precision and accuracy. The results for the reference materials are reported in Table S10, whereas the results for the analysed samples are reported in Table S11.

Data reduction was carried out using the "U-Pb Geochronology" data reduction scheme ("DRS") in Iolite v. 4, with ages calculated and plotted using IsoplotR (Vermeesch, 2018). On-peak gas-blank baselines were fit with an "automatic spline" and subtracted from each channel. Approximately 1 s was trimmed from the beginning and end of the selection of data from each analysis. The GJ-1 zircon was used as the primary standard to correct for drift and downhole fractionation and to normalize 238 U/ 206 Pb and 207 Pb/ 206 Pb. Exponential fits to the downhole fractionation trends were used.

Hafnium isotope compositions of zircons were determined by the same LA-MC-ICP-MS system as the U-Pb analyses, and this was also done at the MiMaC/NGU. A laser beam diameter of 40 µm was used to ablate the previously dated zircon domains, overlapping with the spots ablated for U-Pb determinations. A laser fluence of 4 J cm⁻² and a repetition rate of 9 Hz were used to ablate the grains for 45 s. The ablations were preceded by 35 s gas-blank baselines and followed by 10 s washouts. The ablated aerosol was transported to the MC-ICP-MS in a mixture of He and Ar. Isotopes corresponding to mass / charge ratios of 171-180 were measured in adjacent faraday cups with 10¹¹ W resistors with a 0.1 s integration period. Detailed data reduction procedures are given in Table S12. Results for the primary and secondary standards and for the analysed sample are also given in Tables S13, S14, and S15, respectively.

4 Geology and sulfide mineralization

4.1 Ertelien deposit

The Ertelien deposit is part of an intrusion of approximately $600 \text{ m} \times 500 \text{ m}$, with a rounded shape displaying a slightly E-W elongation (Fig. 1c). The intrusion comprises mainly

a medium-grained gabbronorite with some pegmatite lenses towards the west. The host rock to the intrusion is a granitic gneiss, but the direct relationship between the intrusion and host rock is not well exposed in the field. The main sulfide mineralization is concentrated within the eastern portion of the intrusion (Fig. 1c), with a wider area of disseminated sulfides and massive sulfides along the NE contact between the intrusion and the host gneiss. In the NE portion, a series of old mine excavation pits are found (Fig. 2a). The degree of preservation of magmatic mineralogy and texture in the gabbronorite is variable, and, in some cases, plagioclase, orthopyroxene, and clinopyroxene are well preserved, with pyroxenes displaying a green-brownish colour, whereas plagioclase has a white and clear aspect (Fig. 2b). However, in some cases, both pyroxenes are variably transformed into an amphibole with a darkened colour, and plagioclase becomes greenish and is commonly associated with garnet (Fig. 2c). A similar variation is also observed in the degree of deformation, where undeformed gabbronorite with no clear fabric development is, in some cases, closely associated with strongly deformed equivalents with prominent foliation and no magmatic textures (Fig. 2d). A series of fine-grained mafic dykes are found in the surroundings of the intrusion, displaying a sharp contact with the host gneiss (Fig. 2e). The dykes also display a variable degree of alteration from an assemblage of pyroxene and plagioclase to amphibole and plagioclase (i.e. amphibolite).

In cases where the magmatic assemblage is well preserved, the gabbronorite displays a dominantly adcumulus texture with subhedral orthopyroxene and clinopyroxene crystals in sharp contact with tabular plagioclase (Fig. 2i). Discrete sulfide grains occur interstitially to silicates (Fig. 2j). The degree of alteration is variable but can be observed as a progression from the edges towards the cores of silicates. In the most-preserved cases, discrete amphibole crystals are restricted to the edges and cleavages of pyroxenes (Fig. 2i), and only fine-grained epidote and white mica develop at the contact between pyroxene and plagioclase (Fig. 2k). In more extensively recrystallized cases, pyroxene crystals are rimmed by medium-grained amphibole, and plagioclase displays strong saussuritization (Fig. 21), whereas garnet rims are also observed at the contact between pyroxene and plagioclase (Fig. 2m). In cases of the complete recrystallization of the magmatic assemblage, the rock is a medium-grained amphibolite with granular amphibole and plagioclase. The amphibolite may display no clear preferential deformation (Fig. 2n) or may exhibit a penetrative foliation, typically associated with biotite (Fig. 2o). In some samples, olivine is also observed and commonly occurs as inclusions in larger clinopyroxene crystals (Fig. 2p). In such cases, the rock has a darker aspect and could be referred to as a (olivine-) melanogabbronorite. However, based on our samples and observations, it is not possible to precisely delineate the zones where these olivine-bearing domains occur within the intrusion; still, these do not seem to form continuous layers across the entire intrusion. Although we did not carry out a systematic and detailed petrographic investigation of the host gneiss, in the investigated samples, granular quartz and plagioclase are associated with medium-grained pyrrhotite, commonly elongated parallel to the foliation (Fig. 2q).

The sulfide mineralization is mostly hosted by the medium-grained gabbronorite and varies from disseminated, net-textured, and massive ores, but local brecciated and pegmatoidal ores also occur. Disseminated sulfide is the most widespread texture found within the deposit (Fig. 1c) and comprises interstitial 1-3 mm sulfide blebs around silicates (Fig. 3a), whereas net-textured ores display an interconnection of sulfides forming a framework around silicates (Fig. 3b). In some cases, the net-textured sulfides occur in association with coarse to very coarse-grained silicates, yielding a pegmatoidal aspect (Fig. 3c), but such textures are limited to a few tens of centimetres. In massive ores, the sulfide minerals comprise more than 80 % of the modal proportion, and silicates are present as inclusions within sulfides (Fig. 3d). The massive sulfides locally display a brecciated texture, with angular gabbronorite autholiths occurring within massive sulfide minerals. In these cases, the size and abundance of autholiths are variable, ranging from zones with larger and abundant clasts (Fig. 3e) to zones with fewer clasts of smaller size (Fig. 3f).

In terms of sulfide mineralogy, the assemblage is marked by abundant pyrrhotite, followed by pentlandite and minor chalcopyrite, commonly associated with ilmenite and Ti magnetite (i.e. magnetite with ilmenite exsolution lamellae). In disseminated sulfides, even with the progressive replacement of primary silicates during metamorphism (e.g. pyroxene by amphibole), the interstitial texture of sulfides is preserved (Fig. 3j). In net-textured and massive ores, pentlandite occurs as loops (Fig. 3k) (Barnes et al., 2020; Mansur et al., 2019), commonly around pyrrhotite grains; as exsolution flames within larger pyrrhotite crystals (Fig. 31); or as individual granular crystals (Fig. 3m). Chalcopyrite mainly occurs around the edges of larger pyrrhotite grains (Fig. 3j) or as local accumulations, which can vary from a few millimetres (Fig. 3m) to a few tens of centimetres (Fig. 3e). Pyrite is also an important mineral comprising the sulfide assemblage in all of the ore types. The proportion of pyrite is greater in rocks with a higher degree of alteration. Pyrite is typically medium- to coarse-grained and occurs mainly as euhedral crystals associated with secondary silicates (Fig. 3n). Although the proportion of pyrite is mostly below 15%, in some cases, it can reach up to 40 % (Fig. 3f). Despite the sulfide texture, pyrite tends to develop as an overgrowth over larger pyrrhotite and pentlandite crystals, commonly surrounded by chalcopyrite (Fig. 3n).

4.2 Langedalen deposit

The Langedalen deposit is much smaller than the Ertelien deposit, and the general geology of the deposit is not as

well constrained due to lesser exposure and more structural complexity. The deposit occurs ca. 10 km north of the Ertelien deposit and consists of 1–2 m sulfide lenses that occur within 10-50 m extensively deformed gabbronorite (i.e. in most cases, recrystallized to amphibolite) lenses in contact with a granitic gneiss. The gabbronorite and amphibolite hosting the mineralization display a strong foliation and are constrained to shear zones, with extensive recrystallization of primary mineralogy (Fig. 2f). The gneiss is also marked by a strong plane-parallel foliation, with the local intercalation of centimetre-scale bands richer in plagioclase and quartz with bands richer in amphibole and biotite (Fig. 2g). Several old mine excavation pits are preserved in the area and were developed following the sulfide-rich lenses. In such exposures, it is possible to observe the extensive deformation and confinement of the sulfide lenses within shear zones (Fig. 2h). Although primary textures are not preserved in the Langedalen deposit, it represents an example of an extensively deformed Ni-Cu mineralization and allows for the comparison with the more preserved Ertelien deposit.

In terms of the sulfide mineralization, the sulfide minerals occur either as 5-10 cm veins (Fig. 3g) or as 0.3-1 m lenses of massive sulfides (Fig. 2h). The sulfide mineralogy is marked by the occurrence of pyrrhotite, pentlandite, and chalcopyrite in decreasing proportions, associated with magnetite (Fig. 2h). Some pentlandite textures such as loops and flame exsolutions are preserved (Fig. 3o), as observed in the Ertelien deposit. However, the degree of alteration and the consequent modal proportion of pyrite are much greater in the Langedalen deposit relative to Ertelien. In the deformed sulfide lenses of the Langedalen deposit, pyrite crystals are elongated and crosscut pyrrhotite-rich domains, with a smaller proportion of pentlandite (Fig. 3p). In some cases where pyrite occurs as euhedral crystals, it displays a texture like that observed at Ertelien, and pyrite is in contact with chalcopyrite (Fig. 3q). In the investigated drill core (detailed in the following section), there is the occurrence of a 0.4 m quartz vein displaying a sharp contact with the deformed gabbronorite. This quartz vein contains pyrite, chalcopyrite, and pyrrhotite associated with Au grains. The Au grains vary from 5 to 40 µm in size and occur in contact with pyrite and chalcopyrite or as individual grains within a matrix of quartz \pm biotite and chlorite (Fig. 3r). This quartz vein was only intercepted once in the entire area, and it is thus not possible to discuss its extension. Here, we only explore its occurrence within the deposit from a genetic perspective to provide some constrains regarding mineralization processes.

4.3 Tectonic structures

Subsequent to the formation of the Espedalen and Langedalen Ni deposits, several phases of deformation have affected both the geometry and the extent of the deposits. These tectonic modifications have also affected the two deposits to different extents. The main phase of deformation

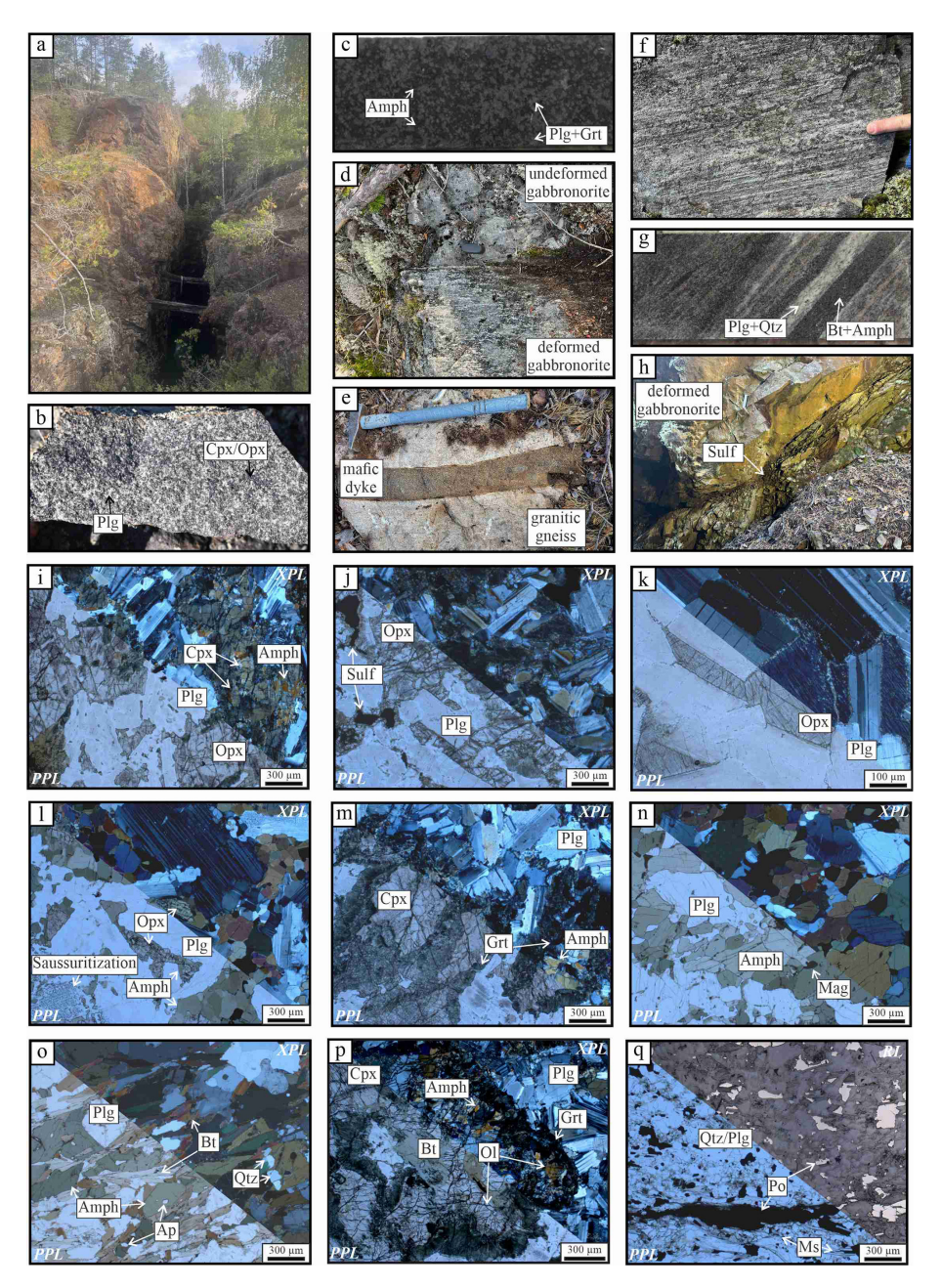


Figure 2. Field and petrographic features of the Ertelien and Langedalen deposits. (a) Old excavation pit at the Ertelien deposit. The opening of the excavation is around 5 m wide. (b) Typical medium-grained gabbronorite from the Ertelien intrusion. (c) Undeformed amphibolite from the Ertelien intrusion with amphibole (replaced pyroxene), plagioclase, and garnet. (d) Sharp contact between undeformed and deformed gabbronorite domains within the Ertelien intrusion. (e) Very fine-grained mafic dyke crosscutting granitic gneiss in the surroundings of the Ertelien intrusion. (f) Deformed gabbronorite with prominent plan parallel foliation from the Langedalen deposit. (g) Banded gneiss with centimetre-scale alternation of zones richer in plagioclase and quartz with zones richer in biotite and amphibole. (h) Sulfide mineralization occurring within a shear zone at the Langedalen deposit. (i) Photomicrograph of adcumulus gabbronorite with subheudral orthopyroxene and clinopyronexe crystals in sharp contact with tabular plagioclase and discrete amphibole in edges and cleavages of pyroxenes. (j) Photomicrograph of gabbronorite with minor interstitial sulfides. (k) Photomicrograph of detail of clinopyroxene exsolutions in orthopyroxene and fine-grained epidote and white-mica developments around plagioclase. (I) Photomicrograph of medium-grained amphibolite with orthopyroxene relict. (m) Photomicrograph of garnet rims that developed at the contact between pyroxene and plagioclase. (n) Photomicrograph of medium-grained amphibolite with no clear mineral fabric. (o) Photomicrograph of medium-grained amphibolite with marked foliation and biotite crystals. (p) Photomicrograph of olivine-bearing gabbronorite, with the development of garnet and amphibole rims at the contact between pyroxene and plagioclase. (q) Photomicrograph of quartz-feldspathic gneiss with elongated pyrrhotite crystals. Abbreviations: Amph - amphibole; Ap - apatite; Bt - biotite; Cpx - clinopyroxene; Grt - garnet; Mag - magnetite; Opx - orthopyroxene; Plg - plagioclase; Qtz quartz; Sulf - sulfide.

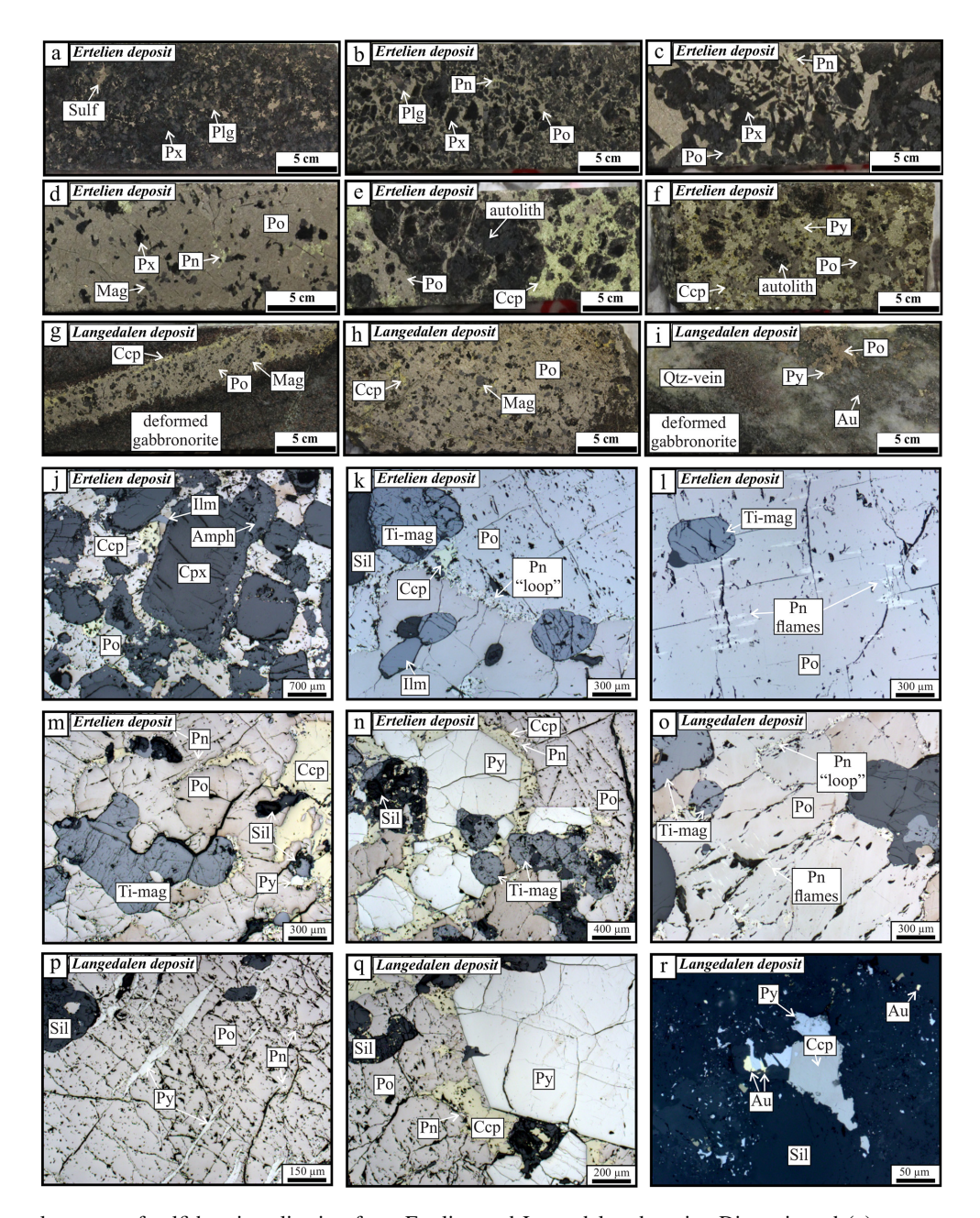


Figure 3. General aspects of sulfide mineralization from Ertelien and Langedalen deposits. Disseminated (a), net-textured (b), pegmatoidal (c), and massive (d) sulfide ores from the Ertelien deposit. The main sulfide minerals are pyrrhotite, pentlandite, and minor chalcopyrite. (e) Semi-massive sulfide with brecciated texture and gabbronorite autolith. Note the chalcopyrite accumulation close to the autolith. (f) Massive sulfide with abundant euhedral pyrite and a few gabbronorite autoliths. (g) Sulfide vein within deformed gabbronorite of the Langedalen deposit. Note the accumulation of chalcopyrite along the margins of the sulfide vein. (h) Massive sulfide from the Langedalen deposit with abundant pyrrhotite, minor chalcopyrite, and rounded magnetite crystals. (i) Au-bearing quartz vein from the Langedalen deposit with associated pyrite and pyrrhotite. The quartz vein crosscuts a deformed gabbronorite. (j) Photomicrograph of disseminated sulfides interstitial to clinopyroxene. Photomicrographs of massive sulfides from Ertelien with pentlandite textures varying from "loop" (k) to exsolution flames (I). (m) Photomicrograph of massive sulfide from Ertelien with pyrrhotite, pentlandite, and chalcopyrite together with rounded Ti magnetite with ilmenite exsolutions. (n) Photomicrograph of massive sulfide from Ertelien with euhedral pyrite crystals surrounded by chalcopyrite. (o) Photomicrograph of massive sulfide from Langedalen with pentlandite "loops" and exsolution flames. (p) Photomicrograph of massive sulfide from Langedalen with anhedral pyrite grains within pyrrhotite. (q) Photomicrograph of massive sulfide from Langedalen with euhedral pyrite together with pyrrhotite, chalcopyrite, and minor pentlandite. (r) Photomicrograph of Au-bearing quartz vein with discrete Au grains occurring either in association with pyrite and chalcopyrite or as minor grains within a silicate matrix. Abbreviations: Amph - amphibole; Ccp - chalcopyrite; Cpx - clinopyroxene; Ilm - ilmenite; Po - pyrrhotite; Pn - pentlandite; Py - pyrite; Ti-mag: Ti magnetite; Qtz – quartz; Sil – silicate; Sulf – sulfide.

affecting the Kongsberg-Modum area was the Sveconorwegian orogen (Bingen et al., 2021; Gorbatschev, 1980; Park et al., 1991; Slagstad et al., 2020; Stephens et al., 1996; Torgersen et al., 2022; Viola et al., 2011; Wahlgren et al., 1994), producing several N-S-oriented tectonic units separated by N-S-trending crustal-scale ductile shear zones (Scheiber et al., 2023; Torgersen et al., 2022; Slagstad et al., 2022; Viola et al., 2011). In the Kongsberg-Modum area, this has resulted in the juxtaposition of tectonic blocks along steeply dipping strike-slip ductile shear zones, the largest of which have been mapped out in detail along the Telmark-Kongsberg and Kongsberg-Modum tectonic contacts (Scheiber et al., 2023). However, smaller, internal shear zones within the Kongsberg-Modum area have not been mapped in detail and, so far, have not been assessed in terms of their effect on the Ni deposits and associated mafic intrusions.

In the Kongsberg-Modum region, we identify internal shear zones from both regional geophysical magnetic data and field observations of major shear zones in the vicinity of both Ertelien and Langedalen. These shear zones are N-S striking and form duplex geometries, suggesting an overall regional dextral displacement (Fig. 4). It is clear from the regional shear zone architecture that the Ertelien deposit does not coincide with an N-S ductile shear zone. This is observed in the field where there is a weak to moderate steeply N-Sdipping foliation but no mineral stretching lineation (Fig. 4a). Therefore, the ductile overprint on the mineralization is negligible. However, the deposit is affected by two sets of brittle structures (Fig. 4a). The first set is parallel to and reactivates the steep N-S foliation, and the second set is perpendicular to the N-S-trending orebody. These cut the mineralization (Fig. 4b) and have an E–W strike–slip displacement (Fig. 4c) of unknown magnitude. The lack of obvious E–W lineations on the regional geophysics may suggest that these are relatively small structures. The Langedalen deposit, however, appears to coincide with a regional-scale N-S ductile shear zone (Fig. 4d). On the margin of the deposit, we observe mylonitic textures in the host rock and intense stretching lineations (Fig. 4e). Indeed, the margin of the deposit appears to be controlled by a N-S-trending, steeply dipping ductile structure. In addition, two sets of brittle structures are also observed (Fig. 4d). An N-S-trending set has strike-slip kinematics, whereas an E-W set has remobilized brecciated ore (Fig. 4g); cutting the N-S deposit geometry shows dip-slip top-to-north kinematics (Fig. 4h) which appear to abruptly delineate the northern margin of the deposit, suggesting a significant displacement. These structures appear to be more significant than those at Ertelien as several regional examples are seen in the geophysics (Fig. 4), suggesting that they are major brittle structures.

5 Results

5.1 Whole-rock geochemistry

Two representative drill cores from the Ertelien deposit (Fig. 5a and b) and one from the Langedalen deposit (Fig. 5c) are investigated here to visualize the main geochemical features of the sulfide mineralization. The drill core ER-2006-05 is 215 m long and intersects with the NE portion of the Ertelien deposit, reaching the host gneiss at ca. 190 m (Fig. 1d). The core comprises an upper interval containing disseminated sulfides for ca. 20 m and a lower interval containing massive sulfides for ca. 10 m. The lower massive sulfide interval is followed downwards by a ca. 30 m interval of melanogabbronorite (Fig. 5a). Some metre-thick sulfide-rich intervals also occur within the host gneiss close to the contact with the intrusion. The drill core ER-2006-06B is 345 m long and also intersects with the NE portion of the Ertelien deposit at a greater depth relative to core ER-2006-05 (Fig. 1d), but it does not reach the host gneiss. The core comprises a relatively homogeneous gabbronorite interval down to ca. 215 m, with a thin pegmatite horizon upwards. The gabbronorite is followed by a sequence of ca. 50 m that contains portions of melanogabbronorite, which hosts a ca. 30 m mineralization interval (Fig. 5b). The mineralized interval comprises disseminated sulfides that shift downwards to massive sulfides, whereas the lower contact of the massive sulfides is with a gneiss xenolith. The drill core LN-07-09 from Langedalen is 173 m long and intersects with a ca. 65 m thick gabbronorite lens within a granitic gneiss. The gabbronorite lens contains disseminated sulfides in the upper portion and a ca. 1 m thick massive sulfide horizon around in its central portion. Above the massive sulfide horizon, there is a ca. 0.4 m Aurich quartz vein (Fig. 5c).

The plot of lithogeochemical results across the drill cores from the Ertelien deposit highlights the intervals with sulfide occurrences, which are marked by a sharp decrease in Mg contents (Fig. 5a and b). The Mg contents vary mainly from 4 wt % to 7 wt % in the gabbronorite and are slightly higher, from 8 wt % to 11 wt %, in the portions containing melanogabbronorite intervals, whereas these drop below 5 wt % in intervals with disseminated sulfides and below 2 wt % in massive sulfides. In contrast, intervals with higher S contents display a positive correlation with Ni, Cu, and Co. Disseminated sulfides yield more than 1 wt % S and Ni, Cu, and Co contents mainly ranging from 0.1 wt % to 0.5 wt %, 0.1 wt % to 0.4 wt %, and 100 to 250 ppm, respectively. Although we delineated the main intervals with disseminated sulfide occurrence, some analyses within the gabbronorite also yield S concentrations close to 1 wt % S, which reflects a fine sulfide dissemination as well. Intervals with massive and net-textured sulfides mostly yield 8 wt % to 30 wt % S and Ni, Cu, and Co contents ranging from 0.5 wt % to 2 wt %, 0.4 wt % to 1.5 wt %, and 400 wt % to 1000 ppm, respectively. The sulfide tenors (i.e. concentrations of met-

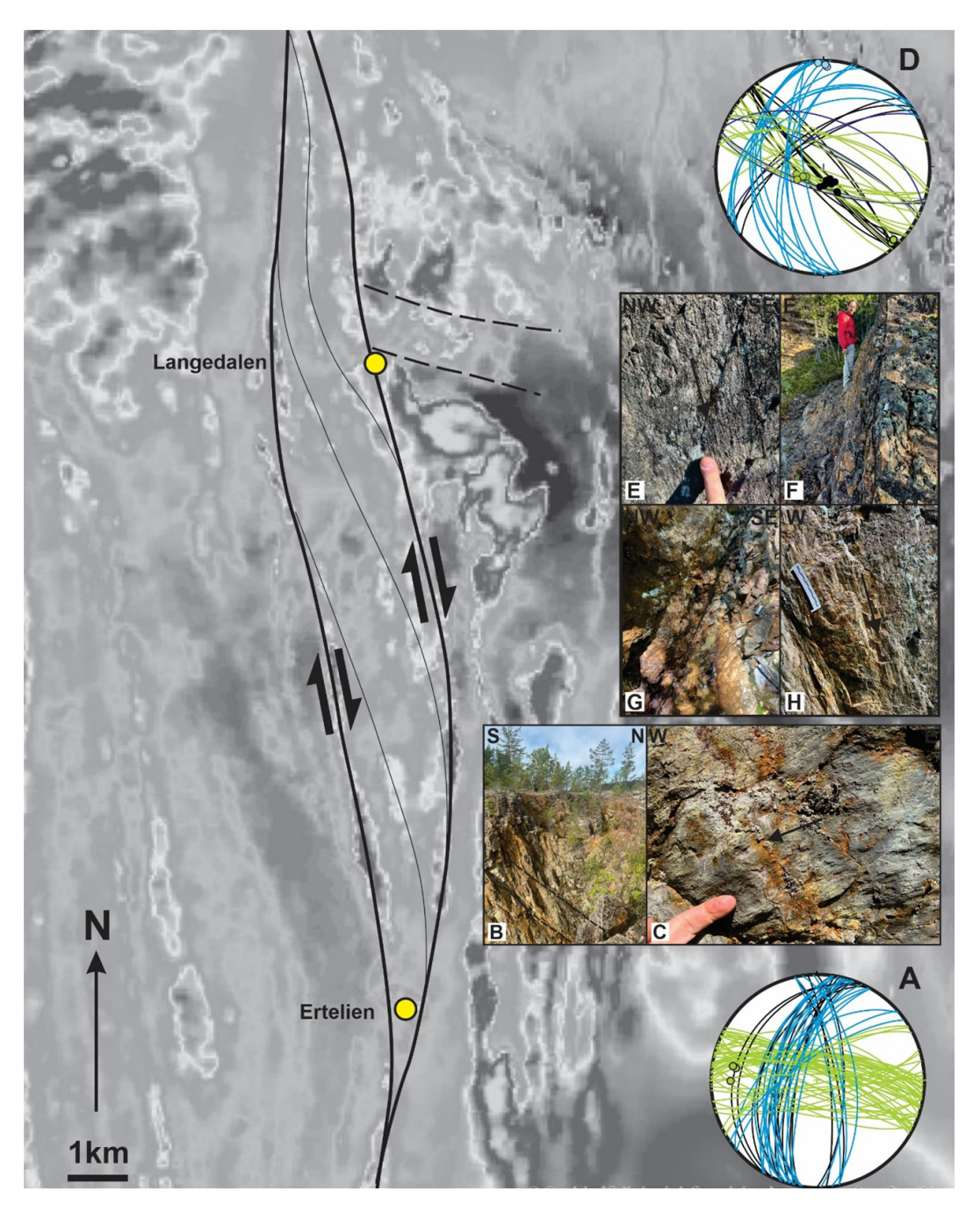


Figure 4. Grey-scale of regional aeromagnetic data with interpreted N–S ductile shear zones (black lines) showing a dextral duplex geometry. Note that the Ertelien deposit is located between shear zones, whereas the Langedalen deposit is located on a shear zone. (a) Stereonet data for the Ertelien deposit. Foliation planes are black. N–S brittle fractures reactivating the foliation are blue, and E–W strike–slip brittle structures are green. (b) E–W brittle structures cutting perpendicularly through the Ertelien deposit. (c) Strike–slip slickensides on the E–W brittle structures. (d) Stereonet data for the Langedalen deposit. Foliation planes are black. N–S brittle fractures reactivating the foliation are blue, and E–W strike–slip brittle structures are green. The E–W brittle structures have two movement episodes: dip–slip and strike–slip. (e) Dip–slip mylonitic mineral stretching lineation on the western margin of the Langedalen deposit. (f) Ductily sheared western margin of the deposit. (g) E–W dip–slip brittle structure with cataclastic fill with sulfides. (h) Dip–slip slickensides showing down-dip displacement of the orebody to the north.

als in cumulus sulfide fraction) obtained from extrapolated metal concentrations up to 35 wt % S (following Barnes et al., 2011) yield Ni, Cu, and Co tenors of ca. 2.2 wt %, 1.5 wt %, and 1200 ppm, respectively. As expected, PGE contents also display a positive correlation with S values; however, concentrations remain very low throughout the Ertelien deposit. Platinum and Pd concentrations are mostly ca. 0.1 ppm in disseminated and massive sulfides. The results across the drill core from the Langedalen deposit are similar to those from Ertelien; however, the sulfide-rich intervals are thinner. Because of the smaller size of sulfide lenses, these are diluted in long core samples, thus yielding lower S concentrations for individual results (Fig. 5c). Nevertheless, the Ni, Cu, and Co tenors are similar to those from the Ertelien deposit.

Because of the low concentrations, the full suite of PGEs was further explored within a subset of samples using better analytical procedures (Table S4). Most of the samples from the Ertelien and Langedalen deposits display similar mantlenormalized Ni, PGE, Au, and Cu patterns, with relatively flat patterns from Ni to Pt, negative Ir anomalies, and a positive slope from Pd to Cu (Fig. 6a). The shapes of the patterns are similar for samples with different sulfide textures; however, there is an increase in magnitude from disseminated sulfides to net-textured and massive sulfides. Values for disseminated sulfides range from 0.01 to 1 times the mantle for iridiumgroup platinum-group elements (IPGE; i.e. Ir, Os, Ru) and up to 20 times the mantle for Cu, whereas values for net-textured and massive sulfide overlap and vary from 0.1 to 10 times the mantle for IPGE and up to 2000 times the mantle for Cu. It is noteworthy that IPGE results are close to or below detection limits of ca. 0.1 ppb in some samples from disseminated sulfides, explaining the negative anomalies. The PGE concentrations in sulfide ores from the Langedalen deposit are similar to those from Ertelien; however, a sample from the Au-rich quartz vein from Langedalen yielded ca. 16 ppm Au, which, although anomalously high, is lower than previously reported (i.e. ca. 150 ppm; Bjerkgård et al., 2020). However, the difference can likely be attributed to a nugget effect in Au concentrations in a small sample where Au is visible; thus, small sampling differences likely yield significant result variations. This sample also has similar PGE concentrations compared to Langedalen sulfides (i.e. from 0.1 to 5 times the mantle), whereas Ni and Cu contents are lower at ca. 0.1 and 10 times the mantle, respectively. A massive sulfide sample from the Langedalen deposit (sample no. 124048, Table S4), which occurs 3 m below the Au-rich quartz vein, also displays a positive Au anomaly with contents of 1000 times the mantle. Lastly, the sample from the mafic dyke near the Ertelien deposit yielded IPGE concentrations below detection limits and Ni and palladium-group platinum-group elements (PPGE; i.e. Pd, Pt and Rh) contents varying from 0.01 to 0.1 times the mantle, whereas Au and Cu concentrations are close to mantle values (Fig. 6a).

Because PGEs and Te, As, Bi, Sb, Sn, and Se (TABS+) are important chalcophile elements for constraining the evo-

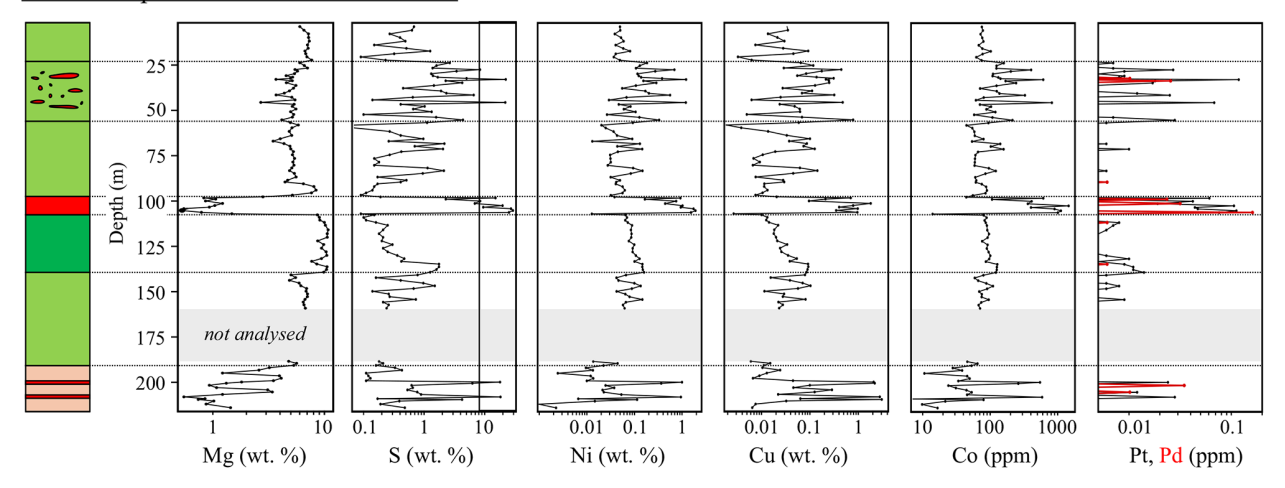
lution of magmatic sulfide deposits, we also present them together using the mantle-normalized diagram proposed by Barnes and Mansur (2022) (Fig. 6b). The elements are arranged in order of partitioning coefficient into a sulfide liquid. Samples from Ertelien have similar Sn contents at 2 to 20 times the mantle, followed by a relatively flat pattern from As to Te, with values ranging from 10 to 50 times the mantle for disseminated sulfides and from 30 to 1000 times the mantle for net-textured and massive sulfides. The pattern is followed by a negative slope to Pt and Pd, with values as described above. Samples of massive sulfides from the Langedalen deposit partially overlap with those from Ertelien. However, the samples from the Au-rich quartz vein and the massive sulfide layer below it (also yielding anomalous Au contents) display positive Sb, Bi, Se, and Te anomalies ranging from 1000 to 10 000 times the mantle (Fig. 6b).

5.2 Trace element composition of base metal sulfides

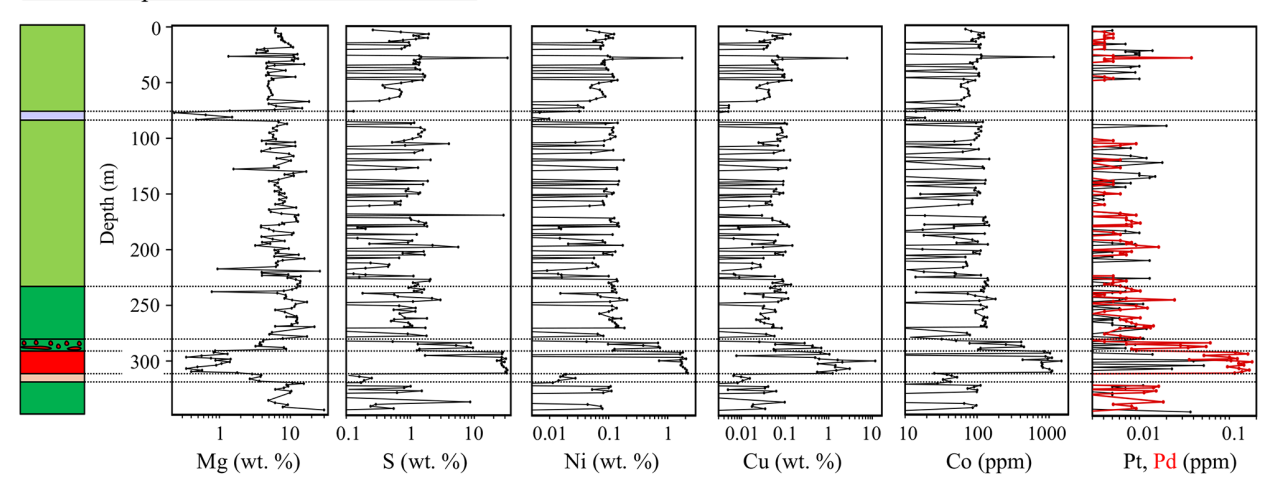
Individual results for concentrations of trace elements in pyrrhotite, pentlandite, chalcopyrite, and pyrite from the Ertelien and Langedalen deposits are reported in Tables S6 to S9, respectively. Typical time-resolved spectra show mostly flat patterns for all of the elements, illustrating their homogeneous distribution within the different sulfide minerals. The time-resolved spectra were also monitored to ensure that inclusions were not included in the integrations when calculating the sulfide compositions.

The concentrations of trace elements in pyrrhotite, pentlandite, chalcopyrite, and pyrite are plotted against Co for better visualization (Fig. 7). This is because Co concentrations in pentlandite and pyrite are the highest, mainly between 1 % and 4 %, followed by pyrrhotite and chalcopyrite, which mainly range from 20 to 1500 and 0.1 to 6 ppm, respectively. The concentrations of different elements in sulfides from disseminated, net-textured, and massive sulfides broadly overlap, along with the composition of sulfides from the Ertelien and Langedalen deposits, with a few exceptions that are explored in the text. Pyrrhotite and chalcopyrite contain from 0.2 % to 3 % and from 2 to 100 ppm Ni, respectively (Fig. 7a), whereas pyrite from Ertelien contains 20 to 300 ppm Ni, and part of those from Langedalen yield higher contents ranging from 0.01 % to 3.5 % Ni. Palladium (Fig. 7b) concentrations are below 0.1 ppm for chalcopyrite and vary from 0.01 to 0.5 ppm in pyrrhotite and pyrite, with the highest values ranging from 0.01 to 2 ppm in pentlandite. Ruthenium contents are mostly below 0.1 ppm in pyrrhotite, chalcopyrite, and pyrite and range between 0.3 to 2 ppm in pentlandite (Fig. 7c). Rhodium concentrations are mostly below detection limits in all sulfides but locally reach ca. 0.2 ppm in pyrite from Ertelien (Fig. 7d). Gold concentrations are below 0.1 ppm in chalcopyrite and pyrrhotite but reach up to ca. 2 ppm in pentlandite and pyrite, except for pyrite from the Au-rich samples of Langedalen, where Au contents in pyrite reach up to 180 ppm (Fig. 7e). Ar-

a Ertelien deposit - drill core ER-2006-05



b Ertelien deposit - drill core ER-2006-06B



c <u>Langedalen deposit - drill core LN-07-09</u>

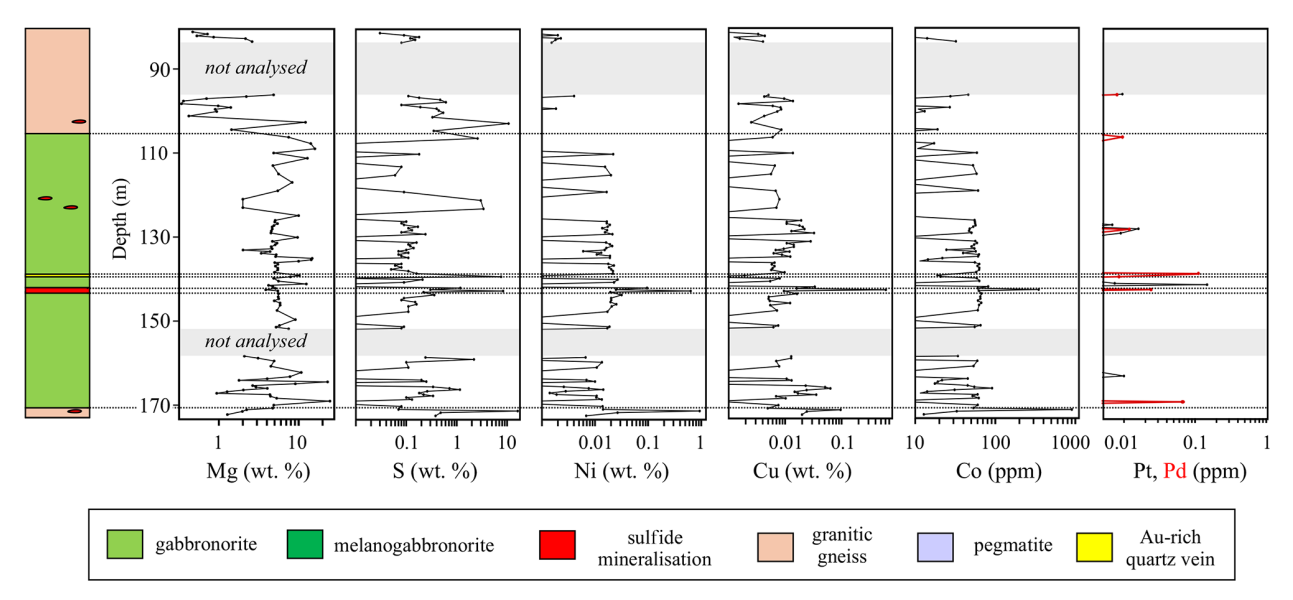


Figure 5. Strip logs and whole-rock Mg, S, Ni, Cu, Co, Pt and Pd results for drill cores (a) ER-2006-05 and (b) ER-2006-06B from the Ertelien deposit and drill core (c) LN-07-09 from the Langedalen deposit. The main lithologies are indicated by solid black lines.

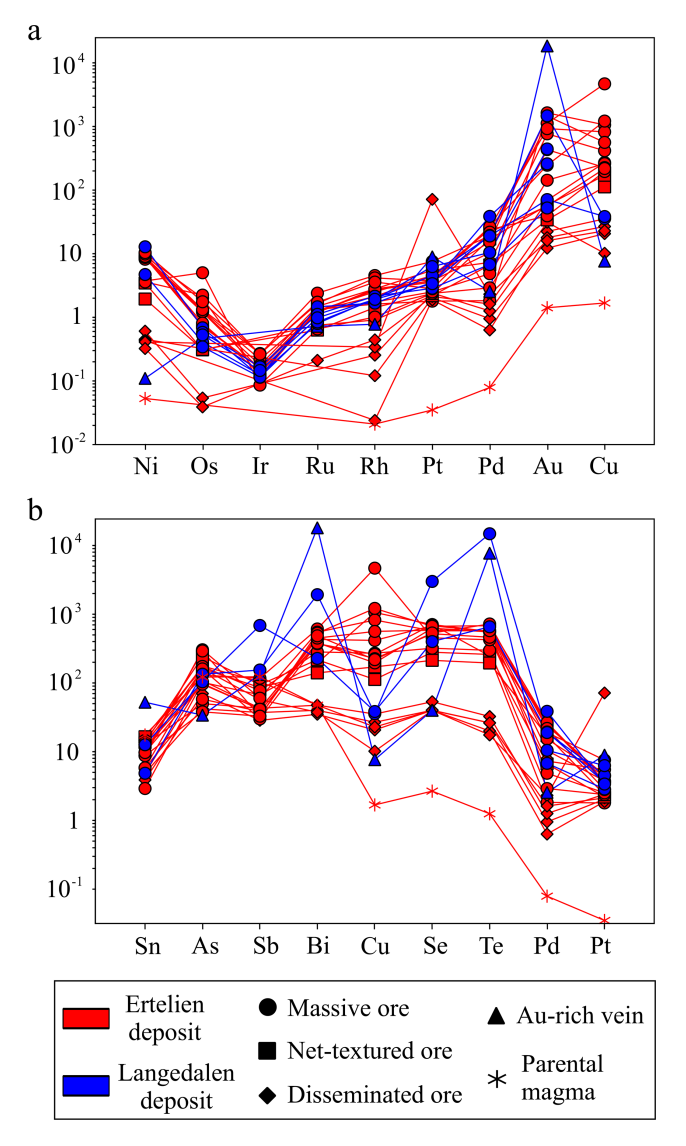


Figure 6. Primitive mantle-normalized **(a)** Ni–PGE–Au-Cu and **(b)** TABS+ patterns of samples from the Ertelien and Langedalen Ni–Cu deposits. Primitive mantle values from Lyubetskaya and Korenaga (2007). Whole-rock results are given in the Supplement, Table S4.

senic, Te, Bi, and Pb (Fig. 7f to h, respectively) display a comparable distribution, with the lowest values mainly overlapping in pyrrhotite and chalcopyrite below 1 ppm for As, below 10 ppm for Te and Bi, and below 50 ppm for Pb. Pentlandite and pyrite have very variable and partially overlapping As, Te, Bi, and Pb concentrations (mostly from 0.1 to 1000 ppm), but the highest values are found in pyrite from the Au-rich quartz vein from Langedalen and are mostly above 1000 ppm. Antimony (Fig. 7j) contents are very scattered and overlap among different sulfides, ranging mostly between 0.05 and 10 ppm, but higher contents, above 100 ppm, are found in pyrite from the Au-rich quartz vein from Langedalen.

Copper concentrations are, as expected, highest in chalcopyrite but range from 1 to 100 ppm in pyrrhotite and pentlandite and are more variable, from 1 to 3300 ppm, in pyrite (Fig. 7k). Zinc, Cd, In, and Sn (Fig. 7l to o, respectively) follow a similar distribution as Cu, with higher concentrations in chalcopyrite, followed by partially overlapping concentrations between pyrrhotite, pentlandite, and pyrite but slightly higher concentrations in pentlandite. These elements broadly overlap between sulfides from Ertelien and Langedalen deposits, except for In concentrations in chalcopyrite, which are the highest in Au-rich quartz vein samples and the underlying massive sulfide lens from Langedalen (Fig. 7n). Silver (Fig. 7p) contents are also very variable and overlap between chalcopyrite, pentlandite, and pyrite, mainly varying from 0.5 to 100 ppm, and are slightly lower between 0.05 and 5 ppm in pyrrhotite. Similarly, as observed from other elements, Ag concentrations in one massive sulfide and the Au-rich quartz vein samples from Langedalen are the highest, reaching up to 1000 ppm. Gallium, Tl, and Mo (Fig. 7q to s, respectively) concentrations vary between 0.01 and 10 ppm and mostly overlap between different sulfides. Although Se (Fig. 7t) contents between different sulfide minerals are similar, these are variable in samples from Ertelien and Langedalen deposits, varying mainly from 30 to 100 ppm in the former and from 200 to 500 ppm in the latter.

The combination of whole-rock and mineral chemistry compositions is commonly used to assess the mass balance of different chalcophile elements in sulfide deposits, thus constraining the mineralogical distribution of the different elements (Barnes et al., 2006; Dare et al., 2010; Godel and Barnes, 2008; Godel et al., 2007; Mansur and Barnes, 2020a; Mansur et al., 2020). However, in the case of our samples for Ertelien and Langedalen deposits, some factors do not allow for a reliable calculation. The concentrations of important elements such as PGE in both whole-rock and mineral analyses are below or close to detection limits. This leads to a scattering of the concentrations, and average concentrations are inaccurate. In addition, the sulfide textures are variable, and our dataset only includes a few samples from each sulfide texture; therefore, grouping samples with different textural relationships in this case would not be appropriate. Also, because of different degrees of alteration in different samples, the pyrite proportion is very variable. Consequently, it is not straightforward to consider such different samples together to arrive at a final mass balance calculation. For these reasons, we opted to not carry out a mass balance calculation to avoid introducing results derived from uncertain calculations into our discussions.

5.3 U-Pb and Hf isotopes

The U-Pb zircon geochronological data for a mediumgrained gabbro-norite of the Ertelien intrusion (sample no. 140388) are shown in Fig. 8a. The obtained age is quoted with 2σ propagated uncertainties. The zircon grains range in

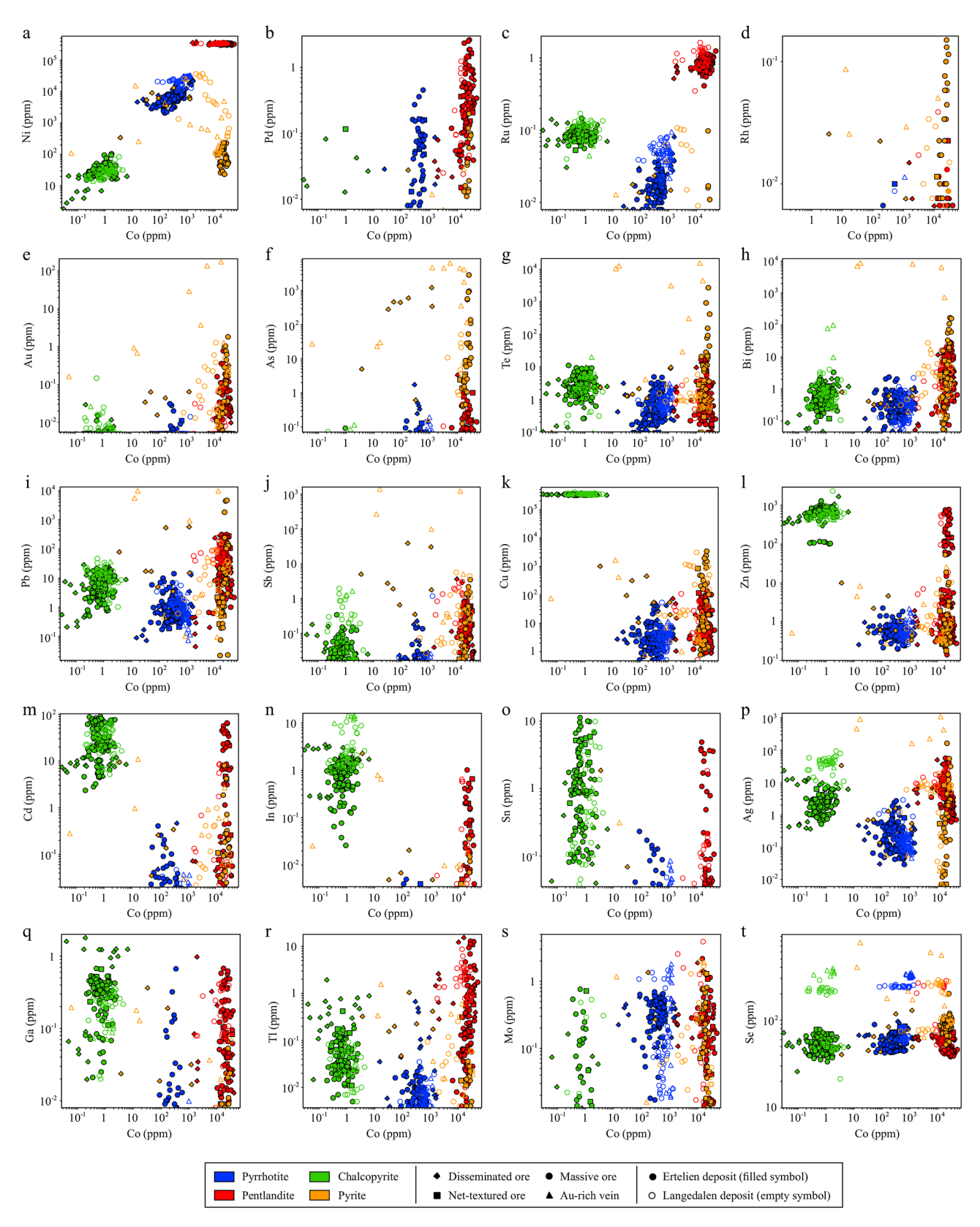


Figure 7. Binary plots of (a) Ni, (b) Pd, (c) Ru, (d) Rh, (e) Au, (f) As, (g) Te, (h) Bi, (i) Pb, (j) Sb, (k) Cu, (l) Zn, (m) Cd, (n) In, (o) Sn, (p) Ag, (q) Ga, (r) Tl, (s) Mo, and (t) Se versus Co for pyrrhotite, pentlandite, chalcopyrite, and pyrite from the Ertelien and Langedalen deposits. The full LA-ICP-MS dataset is given in Tables S6, S7, S8, and S9.

size between 80 and 300 µm and have subrounded, subhedral to euhedral crystal shapes with aspect ratios of between 1:1 and 3:1. Some grains have cores with moderate oscillatory zoning, supporting a magmatic origin. A few grains display darker cores relative to the rim, but no age difference was found in analyses from different crystal zones. We calculated a weighted average $^{207}\text{Pb}/^{206}\text{Pb}$ age of 1559 ± 7 Ma, with 1 rejected outlier out of the total 30 analyses (Fig. 8a), which we interpret here as the crystallization age of the Ertelien intrusion. There is a scattering in some of the analyses, which yield a slightly elevated mean squared weighted deviation (MSWD) of 6.4; however, the analyses were obtained in grains with similar CL textures. Thus, we have no clear explanation for some of the observed scattering, but the obtained age is supported by other geological constraints, as explored further in the text.

Figure 8b shows the in situ Hf isotope analyses from the same zircon crystals where U–Pb analyses were carried out. The initial epsilon Hf (ε Hfi) is calculated relative to crystallization age (Fig. 8a). The results yield ε Hfi varying from 2.9 to 5.2. Two-stage depleted mantle (TDM) model ages calculated relative to a depleted mantle model reservoir with present-day 176 Hf/ 177 Hf = 0.28325 and 176 Lu/ 177 Hf = 0.0384 and a crustal average 176 Lu/ 177 Hf = 0.015 give a TDM of approximately 1.99 Ga (Table S15).

6 Discussion

6.1 Ertelien and Langedalen deposits: magmatic architecture versus tectonic displacement

There is a general consensus that magmatic Ni-Cu(-PGE) sulfide deposits mainly develop as part of long-lived magma pathways where several favourable mechanisms were present (Naldrett, 2004; Barnes et al., 2006; Barnes et al., 2016). For instance, high degrees of mantle partial melting producing primitive magmas, early-stage development within the evolution of a geological province, prolonged magma throughput (in many cases aided by crustal structures), availability of crustal S, favourable reworking, and erosional preservation are some important parameters. Consequently, identifying some of these features is a key step for assessing the mineral potential of a given province and/or a particular intrusion. We explore our findings regarding the Ertelien and Langedalen deposits within a general model for the formation of magmatic sulfide deposits, aiming to constrain both favourable and unfavourable aspects for the prospectivity of magmatic sulfides in the region.

The Ertelien deposit displays some features that are commonly observed in magmatic sulfide deposits worldwide. The intrusion was emplaced within S-bearing gneiss country rocks (Fig. 9a), which represent an external S source to trigger sulfide saturation in a mantle-derived melt rising through the crust (Ripley and Li, 2003, 2013; Lesher, 2017; Keays and Lightfoot, 2010; Lightfoot et al., 2012). Indeed, the main

massive sulfide accumulations are observed at the contact between the intrusion and the host rocks (Fig. 1c), whereas, in some cases, massive sulfides from the Ertelien deposit are found as lenses within the host rocks close to the intrusion. This suggests that S was assimilated upon emplacement of the intrusion, and this external S addition was likely to be the main mechanism triggering S saturation. Moreover, some of the sulfide textures attest to their formation within a dynamic magmatic system (Barnes et al., 2018b). The massive and net-textured sulfides found at the base of the Ertelien deposit (Fig. 9b) are marked by the occurrence of silicate mineral inclusions within a relatively continuous matrix of sulfides (e.g. Fig. 3b and c). Similar textures were also described in the dynamic conduit and funnel-shaped stock of Voisey's Bay and Aguablanca deposits, respectively (Barnes et al., 2017, 2018a). These are proposed to form through sulfide percolation through the pore space of a partially molten silicate rock occurring simultaneously with crystallization, which can be a gravity-driven process (Saumur and Cruden, 2017; Barnes et al., 2018b). Although our dataset does not allow for precise constrainment of the timing of S saturation, the sulfide bodies occur, in some cases, associated with more primitive parts of the intrusion such as melanogabbronorites. This spatial association supports the fact that sulfide saturation occurred relatively early during the formation of the intrusion while the more primitive silicate rocks were crystallizing.

Because our findings support that S saturation at the Ertelien deposit was triggered by external S addition from country rocks, we suggest that the northeastern portion of the intrusion likely represents the base of a tubular intrusion (Fig. 9). In such a scenario, massive sulfides accumulated at the base of the developing intrusive body and were, in some cases, injected into country rocks. Deformation is not pervasive within the deposit, allowing for the identification of preserved magmatic characteristics; however, some features indicate some post-magmatic alteration of the magmatic assemblages. For instance, parts of the silicate rocks were metamorphosed at amphibolite facies, leading to a complete recrystallization in some cases (Fig. 2n and o). Within more altered domains, the sulfide assemblage was also modified, leading to pyrite formation (Fig. 3f, 8c), likely due to Fe loss to surrounding silicates (Holwell et al., 2017; Djon and Barnes, 2012). The formation of secondary pyrite is also a common feature in magmatic sulfide deposits worldwide (Piña et al., 2016; Duran et al., 2015; Piña et al., 2013; Dare et al., 2011) and supports the overprint of post-magmatic fluids. Although constraining the timing of alteration is not straightforward, it is reasonable to assume that it was related to the metamorphic overprint as the degree of metamorphism and sulfide alteration broadly correlate across the deposit. The relative preservation of magmatic textures in the Ertelien deposit is the result of a spatial distribution that is rather distal from the main Sveconorwegian shear zones (Scheiber et al., 2023).

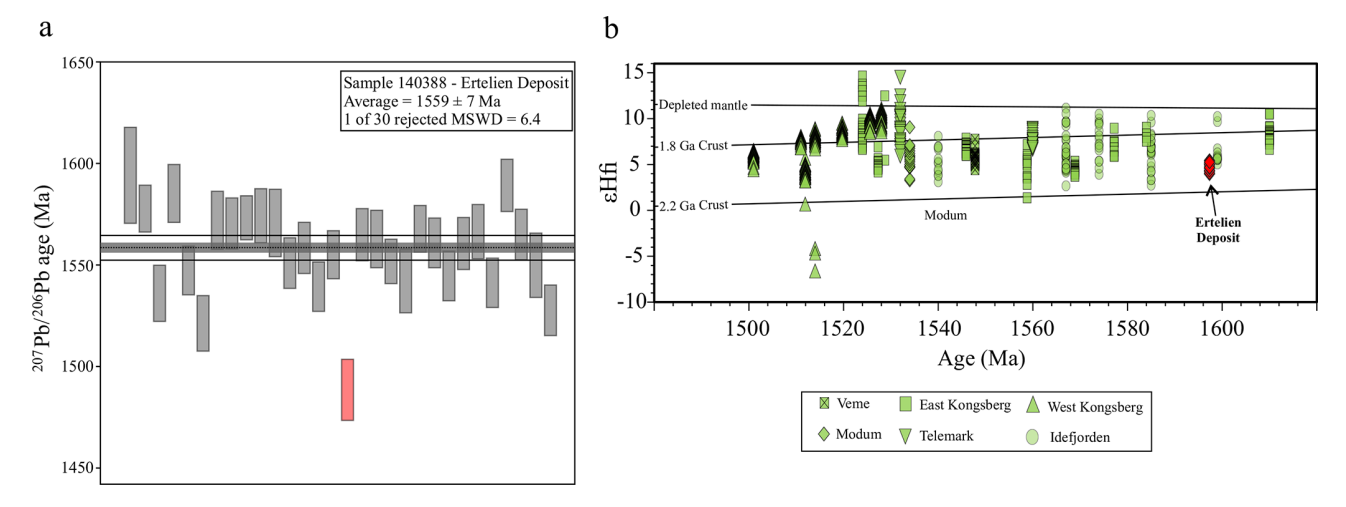


Figure 8. Uranium–Pb and Hf isotope systematics in zircon for sample no. 140388 from the Ertelien intrusion. (a) Weighted average ²⁰⁷Pb/²⁰⁶Pb age, created with IsoplotR (Vermeesch, 2018), with rejected outlier analysis shown in red. (b) Hf isotope evolution plot, with isotope trajectories of the depleted mantle (DM) are shown for reference. Data for Veme, Modum, East Kongsberg, West Kongsberg, and Idefjorden are shown for reference (Slagstad et al., 2024; Orvik et al., 2025).

Although several features from magmatic sulfide deposits can be identified at Ertelien, this is not the case for the Langedalen deposit. There is a clear difference in the overall architecture and sulfide distribution between both deposits. This is consistent with a proximal location of the Langedalen deposit with respect to a regional-scale shear zone (Scheiber et al., 2023) and with the fact that we observe that a mylonitic shear zone forms the western margin of the deposit, most likely resulting in a ductile tectonic attenuation of the deposit. In addition, the deposit appears to be geometrically constrained to the north by significant E-W brittle faults with downthrow towards the north and significant remobilization of the mineralization into cataclastic zones. At the Langedalen deposit, it is not therefore possible to recognize typical features from a previously existing mafic intrusion, and the sulfides are found in lenses constrained to shear zones (Fig. 2h). This could open up the possibility that the Langedalen deposit did not originally represent a magmatic sulfide deposit. Still, the sulfide lenses are mostly hosted by mafic rocks, which may represent fragments of an intrusion. Also, the sulfide mineralogy is typical of magmatic sulfide deposits, comprising pyrrhotite, pentlandite, and chalcopyrite (Fig. 3g and 3h), but displays a more extensive development of secondary pyrite (Fig. 3p). The more extensive degree of alteration and pyrite formation at Langedalen relative to Ertelien is compatible with more extensive deformation and, thus, fluid percolation (Holwell et al., 2017; Mansur et al., 2023c). Another similarity between both the Langedalen and Ertelien deposits is the distribution of trace elements in sulfides, which is comparable, supporting the fact that they originated through similar mechanisms (Fig. 7). This distribution is also similar to those observed in other magmatic sulfide deposits worldwide (Mansur et al., 2021). Fi-

nally, the formation of hydrothermal Ni deposits is mostly accompanied by the development of significant alteration halos within host rocks (Ferreira Filho et al., 2021; Mansur et al., 2023a; González-Álvarez et al., 2013; Le Vaillant et al., 2016, 2015; Keays and Jowitt, 2013), which is not the case at the Langedalen deposit. Thus, we propose that the Langedalen deposit represents a series of tectonically displaced lenses of mafic rocks with associated magmatic sulfides (Fig. 9d).

Based on the main features summarized for the Ertelien and Langedalen deposits, it is possible to argue for the existence of intrusions with different potentials for the formation and preservation of magmatic sulfide deposits within the study area. Intrusions with less deformation and tectonic displacement, such as Ertelien, allow for the partial reconstruction of the magmatic system, display favourable conditions for the development of magmatic sulfides, and can be regarded as fertile. Although the Ertelien deposit is hosted within a relatively small-sized intrusion, this does not necessarily imply a non-fertile system as a high-magma throughput may still take place in such intrusions (Barnes et al., 2016). In contrast, displaced bodies such as the Langedalen deposit are structurally much more complex, and although the mineralization displays similar composition to magmatic sulfides, assessing its extent can be hindered by the structural complexities of the system. The deformation does not rule out the existence of larger occurrences but may create several additional challenges in terms of finding larger orebodies. Still, an interesting similarity between the Ertelien and Langedalen deposits is the PGE-depleted nature of the sulfide mineralization (Fig. 6), which may suggest some genetic link between both systems or a common, PGE-depleted mantle source.

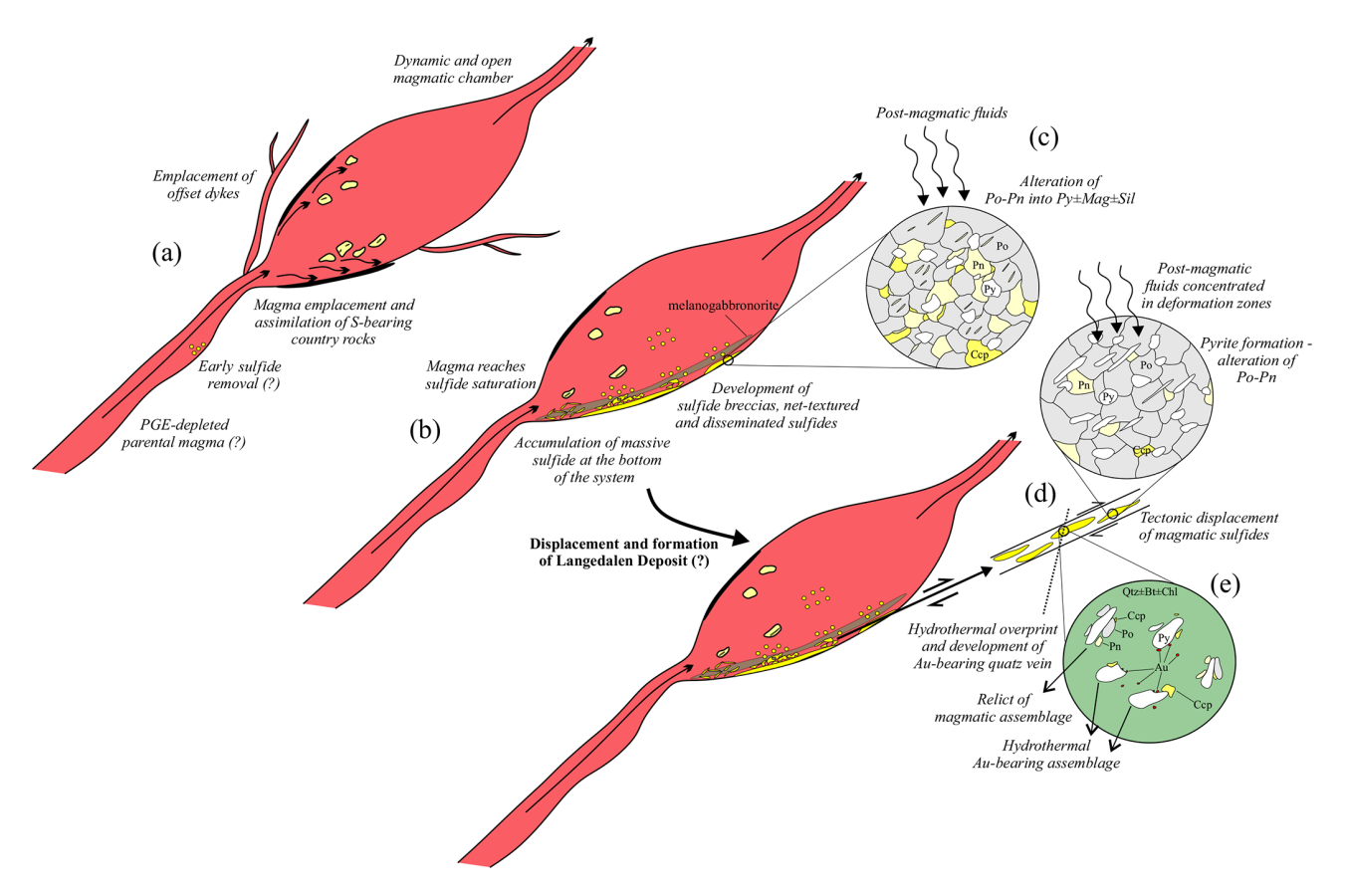


Figure 9. Simplified schematic model showing the steps involved in the formation and remobilization of Ni–Cu sulfides at both the Ertelien and Langedalen deposits. The scale of the intrusion and the degree of displacement of the sulfide bodies are just schematic and cannot be quantified using our data. See the text for further explanation. Abbreviations: Bt – biotite; Ccp – chalcopyrite; Chl – chlorite; Pn – pentlandite; Po – pyrrhotite; Py – pyrite; Qtz – quartz.

6.2 Nature of parent magma and implications for the Ni–Cu mineralization

Constraining the composition of parental magmas in ultramafic-mafic intrusions is an important step to understand the nature of the mantle source, the degree of crustal assimilation, the petrogenesis of the intrusion, and the formation of associated mineral deposits (Latypov et al., 2023; Barnes et al., 2016; Barnes and Lightfoot, 2005). However, assessing the composition of parental magmas is not straightforward as intrusions commonly comprise several cumulate rocks, which do not yield a liquid composition. Therefore, common approaches used to define parental magma compositions include the analogy with chilled margins, bulk wholerock compositions, extrusive equivalents, calculations from cumulus mineral compositions, and investigation of related dykes (Godel et al., 2011; Spandler et al., 2000; Barnes et al., 2010; Wilson, 2012; Mansur and Barnes, 2020b). In the case of the Ertelien intrusion, a series of very fine-grained mafic dykes occur in the vicinity of the intrusion. A recent geochronological study by Orvik et al. (2025) obtained a zircon U-Pb crystallization age of 1584 ± 19 Ma for a mafic dyke near the Ertelien intrusion (sample no. 124723 from this study). This age overlaps with the crystallization age of 1559 ± 7 Ma we obtained for the Ertelien intrusion, and, therefore, it is possible that the composition of this dyke can then be used as an analogue for the composition of parental melts of the Ertelien intrusion. We investigate whether this hypothesis is valid by trying to reproduce the composition of sulfide ores from the Ertelien deposit from the concentration of chalcophile elements in this marginal dyke. Because there are no feasible proxies for parental-melt composition for the Langedalen deposit, we use the same parental-melt candidate to assess the composition of sulfides at Langedalen.

A distinct compositional feature of magmatic sulfides from both the Ertelien and Langedalen deposits is the consistently low PGE contents despite the ore texture (Fig. 6). The occurrence of PGE-depleted magmatic sulfides itself is not unusual and has been observed in several deposits worldwide (Sappin et al., 2011; Sappin et al., 2009; Jesus et al., 2020; Lightfoot et al., 2012; Lu et al., 2019; Mansur et al., 2023b). The most common explanations for their occurrence rely on the highly chalcophile behaviour of PGEs (Liu and Brenan 2015; Mungall and Brenan 2014; Barnes and Rip-

ley 2016), either because of the low degree of partial melting of the mantle leaving sulfide minerals in the source or due to sulfide segregation en route, depleting the magmas (Arndt et al., 2005; Bézos et al., 2005; Song et al., 2011; Lorand et al., 2013). In both cases, the effects of sulfide removal can be assessed by Cu and Pd concentrations because the partition coefficients between a silicate and a coexisting sulfide liquid are in the 10^2 – 10^3 range for Cu and the 10^4 – 10^5 range for Pd (Liu and Brenan, 2015; Mungall and Brenan, 2014; Barnes and Ripley, 2016). Consequently, the removal of small amounts of sulfide liquid significantly decreases Pd contents relative to Cu (Barnes and Maier, 1999). For instance, the marginal mafic dyke from the Ertelien intrusion, also PGE-depleted, has very high Cu/Pd ratios (ca. 80 000) due to low Pd contents (ca. 0.5 ppb; Table S4).

A parental melt produced from approximately 15 % partial melting, or even 10 % (Barnes and Mansur, 2022), would yield PGE contents that are sufficiently high to yield greater tenors than those observed at Ertelien and Langedalen deposits. Therefore, it is not possible to support the hypothesis of low-PGE contents due to a low degree of partial melting of the mantle. In contrast, following a similar approach to that proposed by Lightfoot et al. (2012) for the Voisey Bay deposit, it is possible to broadly reproduce the PGE contents of sulfide from these deposits using a twostage sulfide saturation model (Fig. 10). In such scenario, a parental magma first becomes S-saturated prior to final emplacement, which leads to a depletion in PGEs. The sulfides from both the Ertelien and Langedalen deposits would then form from the second-stage segregation and interaction of this PGE-depleted magma. A similar mechanism has also been proposed for explaining the origin of the PGEdepleted parental from the Romsås deposit (Mansur et al., 2023b), which is located in the Idefjorden LTU and has a similar crystallization age (i.e. $1551 \pm 10 \,\mathrm{Ma}$) compared to the Ertelien and Langedalen deposits. The authors argue that a parental magma that underwent approximately 5 % crystallization with sulfide removal under cotectic proportions is feasible to reproduce the composition of Romsås mineralization. Such magma would have a very similar PGE content to the Ertelien dyke (Fig. 10).

We modelled the PGE and TABS+ concentrations from the Ertelien and Langedalen sulfides using the Ertelien dyke as an analogue for parental-melt composition. The composition of the sulfide liquid was modelled using the equation of Campbell and Naldrett (1979):

$$C_{\text{Sul}} = C_{\text{Sil}} D^{\text{Sul/Sil}} (R+1) / (R+D^{\text{Sul/Sil}}), \tag{1}$$

where $C_{\rm Sul}$ is the concentration of an element in the sulfide liquid, $C_{\rm Sil}$ is the concentration of an element in the silicate liquid, $D^{\rm Sul/Sil}$ is the partition coefficient for the element between sulfide and silicate liquid, and R is the ratio of silicate to sulfide liquid (i.e. R factor). The utilized partition coefficients were 2, 2, 3, 200, 1000, 1000, 5000, and 100 000 for Sn, As, Sb, Bi, Se, Au, Te, and PGE, respectively (Liu and

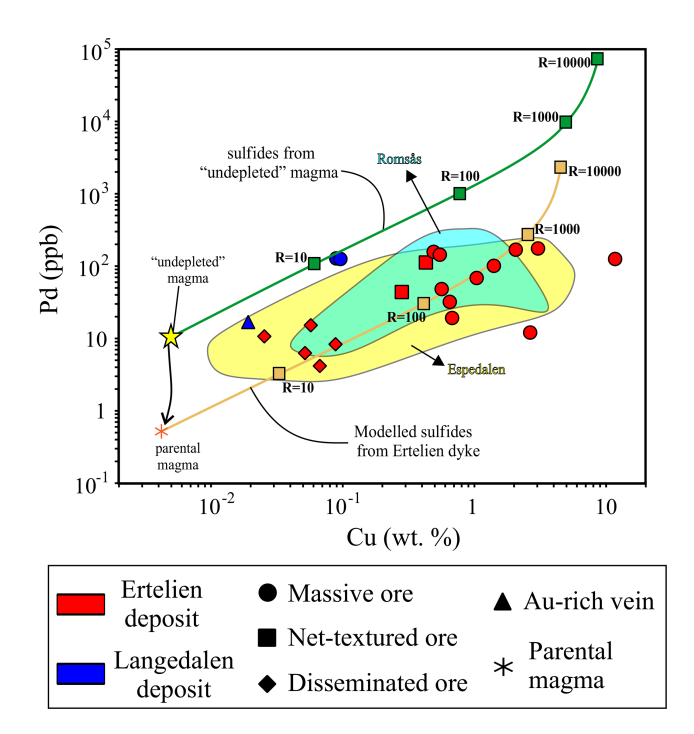


Figure 10. Binary plot of Pd versus Cu for samples from the Ertelien and Langedalen sulfide ores and the sulfide compositional model lines following Lightfoot et al. (2012). Compositional fields for PGE-depleted Ni–Cu sulfide occurrences from Norway are shown for reference: Romsås – Mansur et al. (2023b); Espedalen – Mansur et al. (2023c).

Brenan, 2015; Mungall and Brenan, 2014; Barnes and Ripley, 2016), and the *R* factor was set to 500 based on Cu and Pd estimations (Fig. 10).

The modelled mantle-normalized PGE patterns assuming 25 % to 75 % sulfides closely resemble those from nettextured and massive sulfides from Ertelien and Langedalen deposits, whereas those with 5 % to 10 % sulfides broadly resemble disseminated sulfides (Fig. 11a). However, there are a few slight discrepancies between modelled and observed patterns for IPGE and Pt, especially at low concentrations. One of the possible reasons for this mismatch would be the very low PGE contents and the assumed contents for IPGE in the Ertelien dyke as those were below detection limits. Variables assumed in the model lead to minor absolute differences in obtained values; however, these yield proportionally greater relative differences due to low concentrations. For Pt, a possibility is that a nugget effect may influence Pt contents, leading to positive anomalies in some samples, especially at low concentrations. Another discrepancy is that Cu values are higher in some samples from Ertelien relative to modelled contents, suggesting that either sulfides have fractionated to slightly Cu-rich equivalents in some samples or Cu concentrations from the Ertelien dyke are slightly below realistic values. At this stage, we favour the sulfide fractionation hypothesis as we do observe some Cu-rich portions in

a few of our samples (e.g. Fig. 3e), which could support the fact that such a process took place, at least at a local scale. A broad similarity is also observed between modelled and measured mantle-normalized TABS+ patterns (Fig. 11b). In this case, the main discrepancies are observed in Sn and Bi values, which are higher in modelled patterns relative to what is measured, suggesting that the parental magma had lower Sn and Bi concentrations than the Ertelien dyke. It is noteworthy that similar mismatches in Bi contents were also observed for the Romsås intrusion (Mansur et al., 2023b), but the reasons for this remain not fully understood at this stage.

The content of chalcophile elements in ores from the Langedalen deposit broadly match those from the Ertelien deposit and may thus be modelled assuming a similar parental magma. However, this is not entirely the case for the Au-rich quartz vein and the massive sulfide sample occurring just below it (Figs. 6 and 11b). These samples have a similar content of PGE relative to other sulfide ores; however, they contain much greater concentrations of Bi, Se, Te, and Au, which cannot be accounted for by modelling the segregation of an immiscible sulfide liquid (Fig. 11b). This supports the fact that an additional step must have taken place upon their formation, as will be further explored.

Overall, the composition of sulfide ores from the Ertelien and Langedalen deposits can be reproduced from a parental magma with similar contents of chalcophile elements, especially regarding PGEs, compared to the Ertelien dyke. Although a PGE-depleted composition can be achieved through a two-stage sulfide saturation model, which we cannot rule out as a valid mechanism at this stage, we must also not disregard the possibility that the parental magmas were originally depleted in PGEs and thus did not require sulfide removal prior to emplacement.

6.3 Regional significance of the PGE-depleted signature of magmatic sulfide deposits in southern Norway

The PGE depletion in magmatic Ni-Cu sulfide deposits seems to be a common feature of several occurrences in the southern parts of Norway. The involvement of sulfide removal to produce Ni-fertile parental magmas with low PGE contents partially relies on the mineralogy of the mantle source region. Commonly, Ni-fertile magmas are assumed to be produced upon high-degree partial melting of anhydrous mantle peridotites (Maier and Groves, 2011; Begg et al., 2010), in which olivine is the main host of Ni (Foley et al., 2013), whereas discrete sulfides and alloys host Cu and PGE (Lorand and Luguet, 2016). Consequently, the high-degree partial melting that would be required to sufficiently consume olivine and produce an Ni-rich magma would also melt all of the sulfide components, yielding a PGE-bearing parental magma (Naldrett, 2011; Barnes et al., 2016; Barnes and Lightfoot, 2005). However, the assumption that Ni-fertile parental magmas must be derived from anhydrous mantle peridotites, where olivine is the main host of Ni, has recently been challenged by a close investigation of mantle xenoliths containing a metasomatised assemblage (Blanks et al., 2025). In these xenoliths, Ni is hosted by a range of hydrous minerals such as phlogopite and amphibole, together with olivine and pyroxene. One implication of having a metasomatised mantle source is that Ni-rich magmas could be produced from mantle portions devoid of sulfides or alloys, producing an originally PGE-depleted magma. Moreover, the existence of hydrous metasomatised mantle regions could then control the endowment of Ni deposits within a geological province (Blanks et al., 2025; Ezad et al., 2024).

Another aspect that arises from the discussion regarding hydrous mantle sources leading to the formation of Ni-rich magmas is the wide range of geodynamic settings that may be considered to be fertile for the formation of magmatic Ni-Cu(-PGE) sulfide deposits (Blanks et al., 2025). For instance, magmatic sulfide deposits formed within arc-related or collisional settings are typically PGE-depleted (Jesus et al., 2020; Lu et al., 2019). Some contributions point out that such a geochemical signature may be explained by a pyroxenitic mantle source, produced upon the interaction of recycled oceanic crust with depleted mantle peridotite (Ezad et al., 2024; Blanks et al., 2025). A recent study by Ezad et al. (2024) points out that the contribution of hydrous pyroxenites to the metal endowment of mantle melts may have been previously underestimated. This process is even more critical in subduction and collision zones as the metasomatised mantle regions would be able to re-melt at lower temperatures (Ezad et al., 2024; Foley et al., 2022), still producing Ni-fertile magmas through time.

A scenario of partial melting of metasomatised pyroxenite mantle zones producing parental magmas for mafic intrusions and associated sulfide deposits in the LTUs from southern Norway (i.e. Kongsberg, Idefjorden, Bamble, and Telemark; Fig. 1a) would also be plausible. The widespread mafic magmatism found within these pre-Sveconorwegian LTUs was produced within an arc-related tectonic setting, as highlighted by previous studies (Slagstad et al., 2020; Bingen et al., 2021; Orvik et al., 2025), and a series of PGE-depleted magmatic sulfide occurrences are observed (Sandstad et al., 2012; Barnes et al., 1988). For instance, ε Hfi values from the Ertelien intrusion overlap with those from other intrusions from East Kongsberg and the Idefjorden LTU (Fig. 8b), interpreted to develop as part of a retreating arc system to the west (Orvik et al., 2025). We suggest that the PGE-depleted nature of the magmatic sulfide deposits in the area does not need to be linked to events of sulfide removal prior to the emplacement of the intrusions, although such process cannot be ruled out entirely. Alternatively, the parental magmas that formed these deposits may have been produced upon melting of pyroxenitic mantle domains (Blanks et al., 2025; Ezad et al., 2024). This would be compatible with their formation within a geodynamic setting marked by protracted subduction and recycling of oceanic crust, as supported by previous investigations. Such a hypothesis provides an explanation for

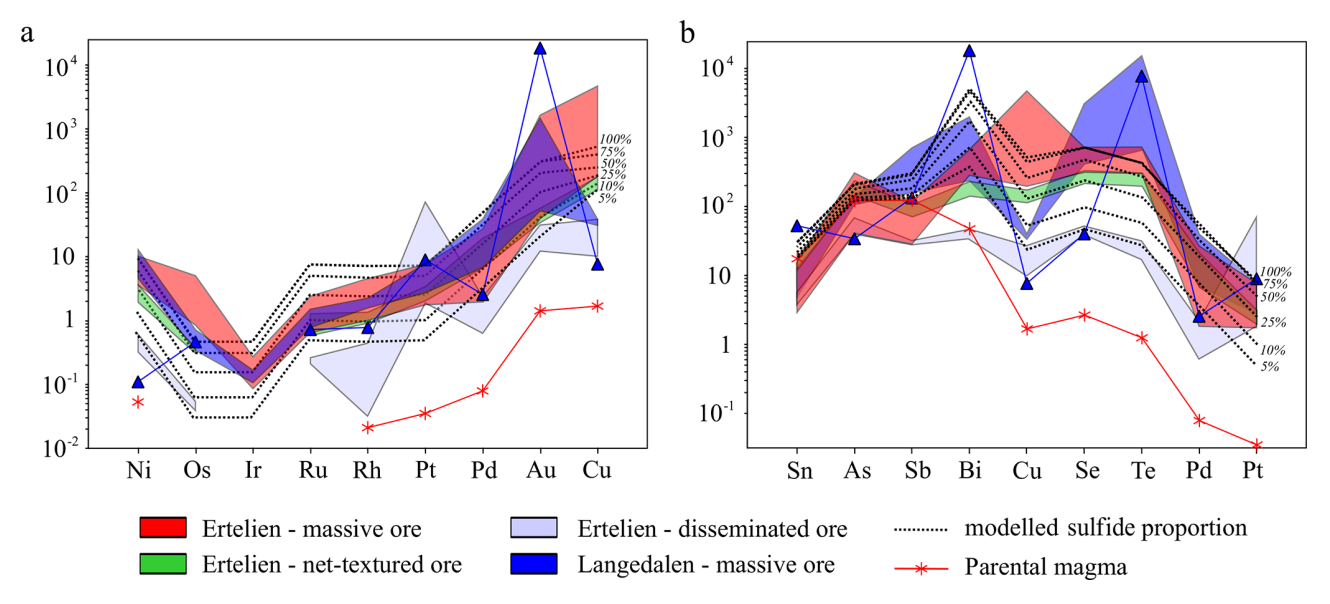


Figure 11. Mantle-normalized (a) Ni–PGE–Au–Cu and (b) TABS+ patterns for parental magma and modelled sulfide composition at different proportions. See the text for a further explanation. Compositional fields of disseminated, net-textured, and massive sulfides from Ertelien and massive sulfides from Langedalen are shown for reference.

the PGE-depleted nature of parental magmas from not only the Ertelien and Langedalen deposits but also other occurrences in southern Norway (Barnes et al., 1988; Mansur et al., 2023b). Moreover, it is possible to envisage that the proposed Ni–Cu metallogenetic provinces in southern Norway (Sandstad et al., 2012) are derived from mantle domains containing a higher proportion of metasomatised hydrous pyroxenite components.

6.4 Hydrothermal overprint following the formation of magmatic sulfide deposits

The composition of sulfide ores from both Ertelien and Langedalen deposits can be broadly reproduced by the segregation of an immiscible sulfide liquid from an evolving silicate magma (Fig. 11). However, sulfide minerals display some degree of alteration, suggesting a post-magmatic percolation of fluids (e.g. Fig. 3p). Moreover, the formation of some of the investigated rocks, such as the Au-rich quartz veins and surrounding massive sulfides from the Langedalen deposit, cannot be attributed solely to magmatic processes. In this section, we explore which compositional features of magmatic sulfides remain preserved and briefly explore hydrothermal processes that formed some of the ores at the Langedalen deposit. The rationale for such an approach is that the concentration of trace elements in magmatic sulfides records a wide range of geological processes (Mansur et al., 2021).

A series of studies propose the use of discriminant diagrams based on sulfide composition to provide petrogenetic constraints for a given mineral deposit (Mansur et al., 2021; Duran et al., 2019, 2016; Caraballo et al., 2022); however,

several limitations were also previously highlighted (Mansur et al., 2023a). For instance, discriminant diagrams rely on the concentration of a few elements, which may lead to misleading classifications. A growing alternative is the use of multivariate statistical methods, which allow us to simultaneously combine a larger number of variables (Caraballo et al., 2022; Sciuba et al., 2020; Miranda et al., 2024, 2022; Makvandi et al., 2016; Bédard et al., 2022). We use our data in some of the available discriminant diagrams for the composition of sulfide minerals to assess whether sulfides from both Ertelien and Langedalen deposits have retained pristine magmatic compositions or if secondary processes such as fluid percolation may have modified their composition.

The sulfides from Ni-Cu deposits have a distinct composition relative to those from PGE-dominated deposits, mainly with regard to the concentration of highly chalcophile elements. Therefore, Duran et al. (2016) proposed the use of Pd and Rh concentrations in pentlandite to discriminate both deposit types (Fig. 12a). As anticipated, pentlandite from the Ertelien deposit plots within the Ni-Cu deposit field overlap with other Ni-Cu deposits in Norway and worldwide. Following a similar approach but using Se, Te, and Bi concentrations, Caraballo et al. (2022) proposed a discriminant diagram for chalcopyrite from Ni-Cu and PGE-dominated deposits (Fig. 12b). Chalcopyrite from the Ertelien deposit plot within the Ni-Cu deposit field is, however, part of the analyses from the Langedalen deposit plot within the field of PGE-dominated deposits, which is a clear misclassification. However, the analyses plotting outside of the Ni-Cu deposit field are from the Au-rich quartz vein and the massive sulfide layer just below, which also display contrasting

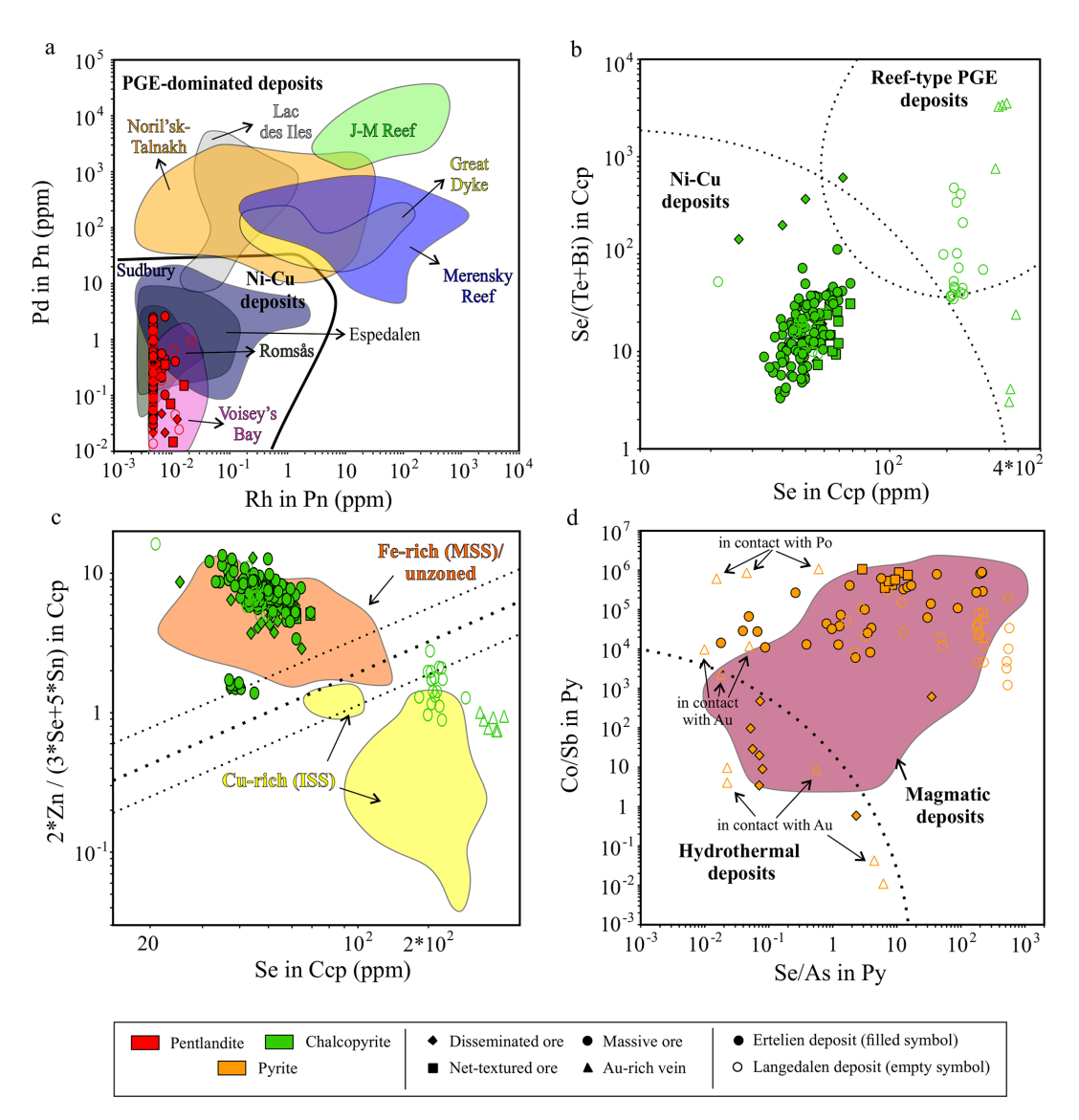


Figure 12. Discriminant diagrams developed for the use of sulfides as petrogenetic indicators. (a) Binary plot of Pd versus Rh in pentlandite (Pn) for differentiating magmatic Ni–Cu and PGE-dominated deposits (Duran et al., 2015). Compositional fields for different magmatic sulfide deposits are compiled by Mansur et al. (2021). (b) Binary plot of Se/(Te+Bi) versus Se in chalcopyrite (Ccp) for differentiating magmatic Ni–Cu and PGE-dominated deposits (Caraballo et al., 2022). (c) Binary plot of $2 \cdot Zn/(3 \cdot Se + 5 \cdot Sn)$ versus Se in chalcopyrite (Ccp) for differentiating Fe-rich and Cu-rich magmatic sulfide deposits (Caraballo et al., 2022). (d) Binary plot of Se/(Sb) versus Se/(Sb) in pyrite (Py) for differentiating magmatic hydrothermal deposits (Duran et al., 2015).

whole-rock compositions relative to the remaining sulfide ores (Fig. 6). The same issue also arises using another discriminant plot for Ni–Cu deposits, which aims to distinguish chalcopyrite compositions from Fe-rich (monosulfide solid solution; MSS-dominated) and Cu-rich (intermediate solid solution; ISS-dominated) portions of deposits using Zn, Se, and Sn contents (Caraballo et al., 2022). Analyses from the Ertelien plot within the Fe-rich compositional field, which is appropriate, whereas the same previously misclassified analyses from the Langedalen deposit plot within the Cu-rich compositional field, which is equivocal (Fig. 12c). The rea-

son for the misclassification arises simply from trying to utilize discriminant diagrams to classify sulfides either with a non-magmatic origin or that had the composition modified by post-magmatic processes (Djon and Barnes, 2012; Holwell et al., 2017; Mansur et al., 2021). This does not invalidate the use of such diagrams but highlights the need to use them with the support of other geological constraints. For instance, it is likely that sulfides from the massive sulfide layer below the Au-rich quartz vein from Langedalen were also affected by the same hydrothermal process leading to its formation, affecting the use of these discriminant diagrams.

Another mineral for which the distribution of trace elements is commonly used to assess different petrogenetic factors is pyrite (Gregory et al., 2015; Genna and Gaboury, 2015; Keith et al., 2016; Steadman et al., 2021; Duran et al., 2015; Piña et al., 2016, 2013). At both the Ertelien and Langedalen deposits, most of the pyrite displays textures typical of alteration of magmatic sulfides, mainly pyrrhotite and pentlandite (Djon and Barnes, 2012; Holwell et al., 2017). In fact, pyrite originating from the alteration of magmatic sulfide commonly displays a distinct composition relative to hydrothermal pyrite, with the former yielding higher IPGE concentrations (i.e. inherited from magmatic sulfides; Duran et al. (2015) and lower concentrations of mobile chalcophile elements (e.g. Se, As, Bi, Sb) (Genna and Gaboury, 2019). Exploring such differences, Duran et al. (2015) proposed a discriminant diagram showing that pyrite from magmatic sulfide deposits (both PGE and Ni-Cu types) is richer in Co and Se and poorer in Sb and As relative to pyrite from hydrothermal deposits. Our data for pyrite from both the Ertelien and Langedalen deposits mainly overlap with the compositional fields for magmatic deposits (Fig. 12d). Pyrite from disseminated sulfides from the Ertelien plot overlap with compositional fields of magmatic and hydrothermal deposits. In the case of the Au-rich quartz vein from the Langedalen deposit, pyrite grains that occur in contact with the pyrrhotite plot within the magmatic deposits field, whereas pyrite grains in contact with Au grains plot within the hydrothermal deposit field (Fig. 12d). This supports the late formation of the Au-rich quartz vein during a hydrothermal overprint event. Still, it is interesting that pyrite grains which are associated with pyrrhotite have a distinct composition closer to that of magmatic grains. This suggests that, although Au was introduced into the system later, together with mobile elements that are high in hydrothermal fluids such as Te, As, Bi, and Sb (Genna and Gaboury, 2019), a part of the magmatic sulfides was also remobilized. This is also confirmed by the modified composition of massive Ni-Cu sulfides near the Au-rich quartz vein in both whole-rock (Fig. 6) and sulfide analyses. However, it is most likely that Te, As, Bi, and Sb were externally added from the hydrothermal fluids and were not simply derived from sulfide mobilization as concentrations are significantly greater in hydrothermal sulfides relative to magmatic sulfides. Although our results allow for an argument for a hydrothermal origin of this local Au-rich quartz vein, partially remobilizing magmatic sulfides, its restricted occurrence, and the number of analyses from our contribution do not allow for a full constrainment of the timing and extent of this Au-mineralizing episode. Still, we strongly encourage further investigations in the area, looking for similar features.

7 Concluding remarks

We have combined field and petrographic observations, whole-rock and sulfide mineral compositions, and U-Pb and Hf isotopic analyses in zircon to investigate the formation of the Ertelien and Langedalen PGE-depleted magmatic sulfide deposits in southern Norway. Our main findings are as follows:

- Zircon U–Pb geochronology yielded a crystallization age of 1559 ± 7 Ma for the Ertelien intrusion, with ε Hfi values varying from 2.9 to 5.2. This age and ε Hfi overlap with those from other intrusions from East Kongsberg and the Idefjorden LTU, which are collectively interpreted as part of a retreating arc system.
- The sulfide mineralization varies from disseminated to net-textured and massive ores in the Ertelien deposit, whereas it comprises mostly massive sulfide lenses in the Langedalen deposit. The mineralogy comprises mainly pyrrhotite followed by pentlandite and minor chalcopyrite, but secondary pyrite is also present and more abundant in extensively altered portions of the mineralization.
- Sulfides from both Ertelien and Langedalen deposits have very low PGE contents, and their composition can be modelled from a PGE-depleted parental magma a with similar composition to that of cogenetic dykes surrounding the intrusion. It is possible that the parental magmas were originally depleted in PGE, thus not requiring sulfide removal prior to emplacement, as commonly argued.
- We suggest that the PGE-depleted nature of the parental magmas that formed the Ertelien and Langedalen deposits may be explained by a metasomatised hydrous pyroxenitic mantle source. This is compatible with the history of protracted subduction and, consequently, the recycling of oceanic crust in the region.
- Sulfide minerals mainly retain their magmatic compositional signature, like those from other magmatic Ni–Cu deposits worldwide. However, part of the sulfides from Langedalen record the effect of hydrothermal overprint, yielding greater contents of mobile elements such as Te, As, Bi, and Sb. This post-magmatic hydrothermal event was also likely to be responsible for the development of an Au-rich quartz vein occurrence at Langedalen.

Data availability. Data used in this study are reported in the Supplement.

Supplement. The supplement related to this article is available online at https://doi.org/10.5194/ejm-37-841-2025-supplement.

Author contributions. EM: conceptualization, investigation, project administration, visualization, writing (original draft preparation). AAO: conceptualization, investigation, writing (original draft preparation). IH: conceptualization, investigation, visualization, writing (original draft preparation). ACM: investigation. TS: conceptualization, writing (original draft preparation). SD: conceptualization, writing (original draft preparation). TB: conceptualization, writing (original draft preparation). JSS: conceptualization, writing (original draft preparation).

Competing interests. The contact author has declared that none of the authors has any competing interests.

Disclaimer. Publisher's note: Copernicus Publications remains neutral with regard to jurisdictional claims made in the text, published maps, institutional affiliations, or any other geographical representation in this paper. While Copernicus Publications makes every effort to include appropriate place names, the final responsibility lies with the authors. Views expressed in the text are those of the authors and do not necessarily reflect the views of the publisher.

Acknowledgements. Parts of the analyses for this study were performed in the Norwegian Laboratory for Mineral and Materials Characterization (MiMaC) NGU node, supported by the Research Council of Norway under project no. 269842/F50. This paper benefited from insightful comments from Xin-Song Wang, José Maria González-Jiménez, and one anonymous reviewer and careful editorial handling by the editors Alessio Langella and Reto Gieré.

Financial support. This research has been supported by the Norges Forskningsråd (grant no. 269842/F50).

Review statement. This paper was edited by Alessio Langella and reviewed by Xinsong Wang, José Maria González-Jiménez, and one anonymous referee.

References

- Åhäll, K.-I. and Connelly, J. N.: Long-term convergence along SW Fennoscandia: 330 my of Proterozoic crustal growth, Precambrian Research, 161, 452–474, 2008.
- Andersen, T., Griffin, W., Jackson, S., Knudsen, T.-L., and Pearson, N.: Mid-Proterozoic magmatic arc evolution at the southwest margin of the Baltic Shield, Lithos, 73, 289–318, 2004.
- Arndt, N. T., Lesher, C. M., and Czamanske, G. K.: Mantle-derived magmas and magmatic Ni-Cu-(PGE) deposits: Economic Geology 100th Anniversary Volume, 5–24, 2005.
- Barnes, S.-J. and Lightfoot, P. C.: Formation of magmatic nickel sulfide deposits and processes affecting their copper and platinum group element contents: Economic Geology, 100th Anniversary Volume, 179–213, 2005.

- Barnes, S.-J. and Maier, W. D.: The fractionation of Ni, Cu and the noble metals in silicate and sulphide liquids, Short Course Notes-Geological Association of Canada, 13, 69–106, 1999.
- Barnes, S.-J. and Mansur, E. T.: Distribution of Te, As, Bi, Sb, and Se in Mid-Ocean Ridge Basalt and Komatiites and in Picrites and Basalts from Large Igneous Provinces: Implications for the Formation of Magmatic Ni-Cu-Platinum Group Element Deposits, Economic Geology, 117, 1919–1933, https://doi.org/10.5382/econgeo.4887, 2022.
- Barnes, S.-J. and Ripley, E. M.: Highly siderophile and strongly chalcophile elements in magmatic ore deposits, Reviews in Mineralogy and Geochemistry, 81, 725–774, 2016.
- Barnes, S.-J., Boyd, R., Korneliussen, A., Nilsson, L., Often, M., Pedersen, R., and Robins, B.: The use of mantle normalization and metal ratios in discriminating between the effects of partial melting, crystal fractionation and sulphide segregation on platinum-group elements, gold, nickel and copper: examples from Norway, Geo-platinum 87, 113–143, 1988.
- Barnes, S.-J., Cox, R. A., and Zientek, M. L.: Platinum-group element, gold, silver and base metal distribution in compositionally zoned sulfide droplets from the Medvezky Creek Mine, Noril'sk, Russia, Contributions to Mineralogy and Petrology, 152, 187–200, 2006.
- Barnes, S.-J., Maier, W. D., and Curl, E. A.: Composition of the Marginal Rocks and Sills of the Rustenburg Layered Suite, Bushveld Complex, South Africa: Implications for the Formation of the Platinum-Group Element Deposits, Economic Geology, 105, 1491–1511, https://doi.org/10.2113/econgeo.105.8.1491, 2010.
- Barnes, S. J., Osborne, G. A., Cook, D., Barnes, L., Maier, W. D., and Godel, B.: The Santa Rita nickel sulfide deposit in the Fazenda Mirabela intrusion, Bahia, Brazil: Geology, sulfide geochemistry, and genesis, Economic Geology, 106, 1083–1110, 2011
- Barnes, S. J., Cruden, A. R., Arndt, N., and Saumur, B. M.: The mineral system approach applied to magmatic Ni–Cu–PGE sulphide deposits, Ore geology reviews, 76, 296–316, 2016.
- Barnes, S. J., Le Vaillant, M., and Lightfoot, P. C.: Textural development in sulfide-matrix ore breccias in the Voisey's Bay Ni-Cu-Co deposit, Labrador, Canada, Ore Geology Reviews, 90, 414–438, 2017.
- Barnes, S. J., Piña, R., and Le Vaillant, M.: Textural development in sulfide-matrix ore breccias in the Aguablanca Ni-Cu deposit, Spain, revealed by X-ray fluorescence microscopy, Ore Geology Reviews, 95, 849–862, 2018a.
- Barnes, S. J., Staude, S., Le Vaillant, M., Piña, R., and Lightfoot, P. C.: Sulfide-silicate textures in magmatic Ni-Cu-PGE sulfide ore deposits: Massive, semi-massive and sulfide-matrix breccia ores, Ore Geology Reviews, 101, 629–651, 2018b.
- Barnes, S. J., Taranovic, V., Schoneveld, L. E., Mansur, E. T., Le Vaillant, M., Dare, S., Staude, S., Evans, N. J., and Blanks, D.: The Occurrence and Origin of Pentlandite-Chalcopyrite-Pyrrhotite Loop Textures in Magmatic Ni-Cu Sulfide Ores, Economic Geology, 115, 1777–1798, https://doi.org/10.5382/econgeo.4757, 2020.
- Bédard, É., de Vazelhes, V. D. B., and Beaudoin, G.: Performance of predictive supervised classification models of trace elements in magnetite for mineral explo-

- ration, Journal of Geochemical exploration, 236, 106959, https://doi.org/10.1016/j.gexplo.2022.106959, 2022.
- Begg, G. C., Hronsky, J. A. M., Arndt, N. T., Griffin, W. L., O'Reilly, S. Y., and Hayward, N.: Lithospheric, Cratonic, and Geodynamic Setting of Ni-Cu-PGE Sulfide Deposits, Economic Geology, 105, 1057–1070, https://doi.org/10.2113/econgeo.105.6.1057, 2010.
- Bézos, A., Lorand, J. P., Humler, E., and Gros, M.: Platinum-group element systematics in Mid-Oceanic Ridge basaltic glasses from the Pacific, Atlantic, and Indian Oceans, Geochimica et Cosmochimica Acta, 69, 2613–2627, https://doi.org/10.1016/j.gca.2004.10.023, 2005.
- Bingen, B. and Viola, G.: The early-Sveconorwegian orogeny in southern Norway: tectonic model involving delamination of the sub-continental lithospheric mantle, Precambrian Research, 313, 170–204, 2018.
- Bingen, B., Birkeland, A., Nordgulen, Ø., and Sigmond, E. M.: Correlation of supracrustal sequences and origin of terranes in the Sveconorwegian orogen of SW Scandinavia: SIMS data on zircon in clastic metasediments, Precambrian Research, 108, 293–318, 2001.
- Bingen, B., Skår, Ø., Marker, M., Sigmond, E. M. O., Nordgulen, Ø., Ragnhildstveit, J., Mansfeld, J., Tucker, R. D., and Liégeois, J.-P.: Timing of continental building in the Sveconorwegian orogen, SW Scandinavia, Norwegian Journal of Geology, 85, 87– 116, 2005.
- Bingen, B., Viola, G., Möller, C., Vander Auwera, J., Laurent, A., and Yi, K.: The Sveconorwegian orogeny, Gondwana Research, 90, 273–313, 2021.
- Bjerkgård, T., Dahlgren, S., Raaness, A., Sandstad, J. S., and Heldal, T.: Mineralressurser i området Kongsberg-Modum-Ringerike, Buskerud, Norwegian Geological Survey (NGU), https://www.ngu.no/publikasjon/mineralressurser-i-omradet-kongsberg-modum-ringerike-buskerud (last access: 31 October 2025) 2020.
- Black, L. P., Kamo, S. L., Allen, C. M., Aleinikoff, J. N., Davis, D. W., Korsch, R. J., and Foudoulis, C.: TEMORA 1: a new zircon standard for Phanerozoic U–Pb geochronology, Chemical geology, 200, 155–170, 2003.
- Blanks, D. E., Holwell, D. A., Ezad, I. S., Giuliani, A., L. Fiorentini, M., and Foley, S. F.: The mineralogical distribution of Ni in mantle rocks controls the fertility of magmatic Ni-sulfide systems, Mineralium Deposita, 60, 1325–1337, https://doi.org/10.1007/s00126-025-01349-9, 2025.
- Boyd, R. and Nixon, F.: Norwegian nickel deposits: a review, Bulletin-Geological survey of Finland, 333, 363–394, 1985.
- Campbell, I. and Naldrett, A.: The influence of silicate: sulfide ratios on the geochemistry of magmatic sulfides, Economic Geology, 74, 1503–1506, 1979.
- Caraballo, E., Dare, S., and Beaudoin, G.: Variation of trace elements in chalcopyrite from worldwide Ni-Cu sulfide and Reef-type PGE deposits: implications for mineral exploration, Mineralium Deposita, 57, 1293–1321, 2022.
- Dare, S. A., Barnes, S.-J., and Prichard, H. M.: The distribution of platinum group elements (PGE) and other chalcophile elements among sulfides from the Creighton Ni-Cu-PGE sulfide deposit, Sudbury, Canada, and the origin of palladium in pentlandite, Mineralium Deposita, 45, 765-793, 2010.

- Dare, S. A., Barnes, S.-J., Prichard, H. M., and Fisher, P. C.: Chalcophile and platinum-group element (PGE) concentrations in the sulfide minerals from the McCreedy East deposit, Sudbury, Canada, and the origin of PGE in pyrite, Mineralium Deposita, 46, 381–407, 2011.
- Djon, M. L. N. and Barnes, S.-J.: Changes in sulfides and platinumgroup minerals with the degree of alteration in the Roby, Twilight, and High Grade Zones of the Lac des Iles Complex, Ontario, Canada, Mineralium Deposita, 47, 875–896, 2012.
- Duran, C. J., Barnes, S. J., and Corkery, J. T.: Chalcophile and platinum-group element distribution in pyrites from the sulfide-rich pods of the Lac des Iles Pd deposits, Western Ontario, Canada: Implications for post-cumulus re-equilibration of the ore and the use of pyrite compositions in exploration, Journal of Geochemical Exploration, 158, 223–242, https://doi.org/10.1016/j.gexplo.2015.08.002, 2015.
- Duran, C. J., Barnes, S. J., and Corkery, J. T.: Trace element distribution in primary sulfides and Fe–Ti oxides from the sulfide-rich pods of the Lac des Iles Pd deposits, Western Ontario, Canada: Constraints on processes controlling the composition of the ore and the use of pentlandite compositions in exploration, Journal of Geochemical Exploration, 166, 45–63, https://doi.org/10.1016/j.gexplo.2016.04.005, 2016.
- Duran, C. J., Dubé-Loubert, H., Pagé, P., Barnes, S.-J., Roy, M., Savard, D., Cave, B. J., Arguin, J.-P., and Mansur, E. T.: Applications of trace element chemistry of pyrite and chalcopyrite in glacial sediments to mineral exploration targeting: Example from the Churchill Province, northern Quebec, Canada, Journal of Geochemical Exploration, 196, 105–130, https://doi.org/10.1016/j.gexplo.2018.10.006, 2019.
- Ezad, I. S., Blanks, D. E., Foley, S. F., Holwell, D. A., Bennett, J., and Fiorentini, M. L.: Lithospheric hydrous pyroxenites control localisation and Ni endowment of magmatic sulfide deposits, Mineralium Deposita, 59, 227–236, https://doi.org/10.1007/s00126-023-01238-z, 2024.
- Ferreira Filho, C. F., Ferraz de Oliveira, M. M., Mansur, E. T., and Rosa, W. D.: The Jaguar hydrothermal nickel sulfide deposit: Evidence for a nickel-rich member of IOCG-type deposits in the Carajás Mineral Province, Brazil, Journal of South American Earth Sciences, 111, 103501, https://doi.org/10.1016/j.jsames.2021.103501, 2021.
- Foley, S. F., Prelevic, D., Rehfeldt, T., and Jacob, D. E.: Minor and trace elements in olivines as probes into early igneous and mantle melting processes, Earth and Planetary Science Letters, 363, 181–191, https://doi.org/10.1016/j.epsl.2012.11.025, 2013.
- Foley, S. F., Ezad, I. S., van der Laan, S. R., and Pertermann, M.: Melting of hydrous pyroxenites with alkali amphiboles in the continental mantle: 1. Melting relations and major element compositions of melts, Geoscience Frontiers, 13, 101380, https://doi.org/10.1016/j.gsf.2022.101380, 2022.
- Genna, D. and Gaboury, D.: Deciphering the hydrothermal evolution of a VMS system by LA-ICP-MS using trace elements in pyrite: an example from the Bracemac-McLeod deposits, Abitibi, Canada, and implications for exploration, Economic Geology, 110, 2087–2108, 2015.
- Genna, D. and Gaboury, D.: Use of semi-volatile metals as a new vectoring tool for VMS exploration: Example from the Zn-rich McLeod deposit, Abitibi, Canada,

- Journal of Geochemical Exploration, 207, 106358, https://doi.org/10.1016/j.gexplo.2019.106358, 2019.
- Godel, B. and Barnes, S.-J.: Platinum-group elements in sulfide minerals and the whole rocks of the JM Reef (Stillwater Complex): Implication for the formation of the reef, Chemical Geology, 248, 272–294, 2008.
- Godel, B., Barnes, S.-J., and Maier, W. D.: Platinum-group elements in sulphide minerals, platinum-group minerals, and whole-rocks of the Merensky Reef (Bushveld Complex, South Africa): implications for the formation of the reef, Journal of Petrology, 48, 1569–1604, 2007.
- Godel, B., Barnes, S.-J., and Maier, W. D.: Parental magma composition inferred from trace element in cumulus and intercumulus silicate minerals: an example from the Lower and Lower Critical Zones of the Bushveld Complex, South-Africa, Lithos, 125, 537–552, 2011.
- González-Álvarez, I., Pirajno, F., and Kerrich, R.: Hydrothermal nickel deposits: Secular variation and diversity, Ore Geology Reviews, 52, 1–3, 2013.
- Gorbatschev, R.: The Precambrian development of southern Sweden, Geologiska Föreningen i Stockholm Förhandlingar, 102, 129–136, 1980.
- Gregory, D. D., Large, R. R., Halpin, J. A., Baturina, E. L., Lyons, T. W., Wu, S., Danyushevsky, L., Sack, P. J., Chappaz, A., and Maslennikov, V. V.: Trace element content of sedimentary pyrite in black shales, Economic Geology, 110, 1389–1410, 2015.
- Griffin, W., Begg, G., and O'reilly, S. Y.: Continental-root control on the genesis of magmatic ore deposits, Nature Geoscience, 6, 905–910, 2013.
- Holwell, D. A., Adeyemi, Z., Ward, L. A., Smith, D. J., Graham, S. D., McDonald, I., and Smith, J. W.: Low temperature alteration of magmatic Ni-Cu-PGE sulfides as a source for hydrothermal Ni and PGE ores: A quantitative approach using automated mineralogy, Ore Geology Reviews, 91, 718–740, 2017.
- Jackson, S. E., Pearson, N. J., Griffin, W. L., and Belousova, E. A.: The application of laser ablation-inductively coupled plasmamass spectrometry to in situ U–Pb zircon geochronology, Chemical geology, 211, 47–69, 2004.
- Jesus, A. P., Mateus, A., Benoit, M., Tassinari, C. C. G., and Bento dos Santos, T.: The timing of sulfide segregation in a Variscan synorogenic gabbroic layered intrusion (Beja, Portugal): Implications for Ni-Cu-PGE exploration in orogenic settings, Ore Geology Reviews, 126, 103767, https://doi.org/10.1016/j.oregeorev.2020.103767, 2020.
- Jochum, K. P., Nohl, U., Herwig, K., Lammel, E., Stoll, B., and Hofmann, A. W.: GeoReM: a new geochemical database for reference materials and isotopic standards, Geostandards and Geoanalytical Research, 29, 333–338, 2005.
- Keays, R. R. and Jowitt, S. M.: The Avebury Ni deposit, Tasmania: A case study of an unconventional nickel deposit, Ore Geology Reviews, 52, 4–17, 2013.
- Keays, R. R. and Lightfoot, P. C.: Crustal sulfur is required to form magmatic Ni–Cu sulfide deposits: evidence from chalcophile element signatures of Siberian and Deccan Trap basalts, Mineralium deposita, 45, 241–257, 2010.
- Keith, M., Häckel, F., Haase, K. M., Schwarz-Schampera, U., and Klemd, R.: Trace element systematics of pyrite from submarine hydrothermal vents, Ore Geology Reviews, 72, 728–745, 2016.

- Kuniko: 23Mt Mineral Resource Estimate for Ertelien Unveils Sustainable Nickel & Copper Potential, Australian Securities Exchange, ASX, Kuniko, https://kuniko.eu/asx-announcements/ (last access: 31 October 2025), 2024.
- Latypov, R. M., Namur, O., Bai, Y., Barnes, S. J., Chistyakova, S., Holness, M. B., Iacono-Marziano, G., Kruger, W. A., O'Driscoll, B., and Smith, W. D.: Layered intrusions: Fundamentals, novel observations and concepts, and controversial issues, Earth-Science Reviews, 104653, https://doi.org/10.1016/j.earscirev.2023.104653, 2023.
- Lesher, C.: Roles of xenomelts, xenoliths, xenocrysts, xenovolatiles, residues, and skarns in the genesis, transport, and localization of magmatic Fe-Ni-Cu-PGE sulfides and chromite, Ore Geology Reviews, 90, 465–484, 2017.
- Le Vaillant, M., Barnes, S. J., Fiorentini, M. L., Miller, J., Mc-Cuaig, T. C., and Muccilli, P.: A hydrothermal Ni-As-PGE geochemical halo around the Miitel komatiite-hosted nickel sulfide deposit, Yilgarn Craton, Western Australia, Economic Geology, 110, 505–530, 2015.
- Le Vaillant, M., Saleem, A., Barnes, S. J., Fiorentini, M. L., Miller, J., Beresford, S., and Perring, C.: Hydrothermal remobilisation around a deformed and remobilised komatiite-hosted Ni-Cu-(PGE) deposit, Sarah's Find, Agnew Wiluna greenstone belt, Yilgarn Craton, Western Australia, Mineralium Deposita, 51, 369–388, 2016.
- Lightfoot, P. C., Keays, R. R., Evans-Lamswood, D., and Wheeler, R.: S saturation history of Nain Plutonic Suite mafic intrusions: origin of the Voisey's Bay Ni–Cu–Co sulfide deposit, Labrador, Canada, Mineralium Deposita, 47, 23–50, 2012.
- Liu, Y. and Brenan, J.: Partitioning of platinum-group elements (PGE) and chalcogens (Se, Te, As, Sb, Bi) between monosulfide-solid solution (MSS), intermediate solid solution (ISS) and sulfide liquid at controlled fO2–fS2 conditions, Geochimica et Cosmochimica Acta, 159, 139–161, https://doi.org/10.1016/j.gca.2015.03.021, 2015.
- Lorand, J.-P. and Luguet, A.: Chalcophile and Siderophile Elements in Mantle Rocks: Trace Elements Controlled By Trace Minerals, Reviews in Mineralogy and Geochemistry, 81, 441–488, https://doi.org/10.2138/rmg.2016.81.08, 2016.
- Lorand, J.-P., Luguet, A., and Alard, O.: Platinum-group element systematics and petrogenetic processing of the continental upper mantle: A review, Lithos, 164–167, 2–21, https://doi.org/10.1016/j.lithos.2012.08.017, 2013.
- Lu, Y., Lesher, C. M., and Deng, J.: Geochemistry and genesis of magmatic Ni-Cu-(PGE) and PGE-(Cu)-(Ni) deposits in China, Ore Geology Reviews, 107, 863–887, 2019.
- Lyubetskaya, T. and Korenaga, J.: Chemical composition of Earth's primitive mantle and its variance: 1. Method and results, Journal of Geophysical Research: Solid Earth, 112, https://doi.org/10.1029/2005JB004223, 2007.
- Maier, W. D. and Groves, D. I.: Temporal and spatial controls on the formation of magmatic PGE and Ni–Cu deposits, Mineralium Deposita, 46, 841–857, https://doi.org/10.1007/s00126-011-0339-6, 2011.
- Makvandi, S., Ghasemzadeh-Barvarz, M., Beaudoin, G., Grunsky, E. C., McClenaghan, M. B., Duchesne, C., and Boutroy, E.: Partial least squares-discriminant analysis of trace element compositions of magnetite from various VMS deposit subtypes: Applica-

- tion to mineral exploration, Ore Geology Reviews, 78, 388–408, 2016
- Mansur, E. T. and Barnes, S.-J.: The role of Te, As, Bi, Sn and Sb during the formation of platinum-group-element reef deposits: Examples from the Bushveld and Stillwater Complexes, Geochimica et Cosmochimica Acta, 272, 235–258, https://doi.org/10.1016/j.gca.2020.01.008, 2020a.
- Mansur, E. T. and Barnes, S.-J.: Concentrations of Te, As, Bi, Sb and Se in the Marginal Zone of the Bushveld Complex: Evidence for crustal contamination and the nature of the magma that formed the Merensky Reef, Lithos, 358–359, 105407, https://doi.org/10.1016/j.lithos.2020.105407, 2020b.
- Mansur, E. T., Barnes, S.-J., and Duran, C. J.: Textural and compositional evidence for the formation of pentlandite via peritectic reaction: Implications for the distribution of highly siderophile elements, Geology, 47, 351–354, https://doi.org/10.1130/g45779.1, 2019.
- Mansur, E. T., Barnes, S.-J., Duran, C. J., and Sluzhenikin, S. F.: Distribution of chalcophile and platinum-group elements among pyrrhotite, pentlandite, chalcopyrite and cubanite from the Noril'sk-Talnakh ores: implications for the formation of platinum-group minerals, Mineralium Deposita, 55, 1215–1232, https://doi.org/10.1007/s00126-019-00926-z, 2020.
- Mansur, E. T., Barnes, S.-J., and Duran, C. J.: An overview of chalcophile element contents of pyrrhotite, pentlandite, chalcopyrite, and pyrite from magmatic Ni-Cu-PGE sulfide deposits, Mineralium Deposita, 56, 179–204, 2021.
- Mansur, E. T., Dare, S. A. S., Filho, C. F. F., Miranda, A. C. R., and Monteiro, L. V. S.: The distribution of trace elements in sulfides and magnetite from the Jaguar hydrothermal nickel deposit: Exploring the link with IOA and IOCG deposits within the Carajás Mineral Province, Brazil, Ore Geology Reviews, 152, 105256, https://doi.org/10.1016/j.oregeorev.2022.105256, 2023a.
- Mansur, E. T., Sandstad, J. S., Slagstad, T., Miranda, A. C. R., Dare, S. A. S., and Nilsson, L. P.: Geology, sulphide geochemistry and geochronology of the Romsås Ni-Cu-Co mineralisation, Norway: Implications for ore formation and regional prospectivity, Lithos, 454–455, 107244, https://doi.org/10.1016/j.lithos.2023.107244, 2023b.
- Mansur, E. T., Slagstad, T., Dare, S. A. S., and Sandstad, J. S.: Geology and sulphide geochemistry of the Ni-Cu-Co mineralisation of the Espedalen Complex, Norway: Constraints for the distribution of magmatic sulphides within a variably deformed anorthosite suite, Ore Geology Reviews, 161, 105666, https://doi.org/10.1016/j.oregeorev.2023.105666, 2023c.
- Mathiesen, C. O.: Vurdering av Ringerike nikkelfelter, Norges Geologiske Undersøkelse, Norway, Norwegian Geological Survey (NGU), 21, https://www.ngu.no/publikasjon/vurdering-av-ringerike-nikkelfelter (last access: 31 October 2025), 1977.
- Miranda, A. C. R., Beaudoin, G., and Rottier, B.: Scheelite chemistry from skarn systems: implications for ore-forming processes and mineral exploration, Mineralium Deposita, 57, 1469–1497, 2022.
- Miranda, A. C. R., Beaudoin, G., Rottier, B., Pašava, J., Bohdálek, P., and Malec, J.: Trace element signatures in Scheelite associated with various deposit types: a tool for mineral targeting, Journal of Geochemical Exploration, 266, 107555, https://doi.org/10.1016/j.gexplo.2024.107555, 2024.

- Mungall, J. E. and Brenan, J. M.: Partitioning of platinum-group elements and Au between sulfide liquid and basalt and the origins of mantle-crust fractionation of the chalcophile elements, Geochimica et Cosmochimica Acta, 125, 265–289, https://doi.org/10.1016/j.gca.2013.10.002, 2014.
- Munz, I. A., Wayne, D., and Austrheim, H.: Retrograde fluid infiltration in the high-grade modum complex South Norway: evidence for age, source and REE mobility, Contributions to Mineralogy and Petrology, 116, 32–46, 1994.
- Naldrett, A. J.: Fundamentals of Magmatic Sulfide Deposits, in: Magmatic Ni-Cu and PGE Deposits: Reviews in Economic Geology, 17, 1–50, https://doi.org/10.5382/Rev.17.01, 2011.
- Naldrett, A. J.: Magmatic sulfide deposits: geology, geochemistry and exploration, Springer, Berlin, 727 pp., 2004.
- Niarezka, A.: A Petrographic and Paragenetic Characterization of the Ertelien Ni-Cu Deposit (Norway), M.Sc. thesis, ISSN 1650-6553, 57 pp., 2023.
- Orvik, A. A., Mansur, E. T., Henderson, I., Slagstad, T., Huyskens, M., and Bjerkgård, T.: Isotopic identification of paleo rift zones within the Sveconorwegian Province; implications for nickel sulphide mineralisations in the SW Fennoscandian Shield, Precambrian Research, 427, 107836, https://doi.org/10.1016/j.precamres.2025.107836, 2025.
- Park, R., Åhäll, K.-I., and Bland, M.: The Sveconorwegian shear-zone network of SW Sweden in relation to mid-Proterozoic plate movements, Precambrian Research, 49, 245–260, 1991.
- Patton, C., Hellstrom, J., Paul, B., Woodhead, J. H., and Hergt, J.: Iolite: freeware for the visualization and processing of mass spectrometry data, Journal of Analytical Atomic Spectrometry, 26, 2508–2518, 2011.
- Piña, R., Gervilla, F., Barnes, S.-J., Ortega, L., and Lunar, R.: Platinum-group elements-bearing pyrite from the Aguablanca Ni-Cu sulphide deposit (SW Spain): A LA-ICP-MS study, European Journal of Mineralogy, 25, 241–252, 2013.
- Piña, R., Gervilla, F., Barnes, S.-J., Oberthür, T., and Lunar, R.: Platinum-group element concentrations in pyrite from the Main Sulfide Zone of the Great Dyke of Zimbabwe, Mineralium Deposita, 51, 853–872, 2016.
- Reddick, J. and Armstrong, T.: Technical Report on Resource Estimates for the Ertelien, Stormyra and Dalen Deposits, Southern Norway, Reddick Consulting Inc, BLACKSTONE VENTURES INC., Uppsala University, Disciplinary Domain of Science and Technology, Earth Sciences, Department of Earth Sciences, 58 pp., 2009.
- Ripley, E. M. and Li, C.: Sulfur isotope exchange and metal enrichment in the formation of magmatic Cu-Ni-(PGE) deposits, Economic Geology, 98, 635–641, 2003.
- Ripley, E. M. and Li, C.: Sulfide saturation in mafic magmas: Is external sulfur required for magmatic Ni-Cu-(PGE) ore genesis?, Economic geology, 108, 45–58, 2013.
- Roberts, N. M. and Slagstad, T.: Continental growth and reworking on the edge of the Columbia and Rodinia supercontinents; 1.86–0.9 Ga accretionary orogeny in southwest Fennoscandia, International Geology Review, 57, 1582–1606, 2015.
- Roberts, N. M., Slagstad, T., Parrish, R. R., Norry, M. J., Marker, M., and Horstwood, M. S.: Sedimentary recycling in arc magmas: geochemical and U–Pb–Hf–O constraints on the Mesoproterozoic Suldal Arc, SW Norway, Contributions to Mineralogy and Petrology, 165, 507–523, 2013.

- Sandstad, J., Bjerkgård, T., Boyd, R., Ihlen, P., Korneliussen, A., Nilsson, L., Often, M., Eilu, P., and Hallberg, A.: Metallogenic areas in Norway, Mineral deposits and metallogeny of Fennoscandia (P. Eilu Ed.), Geological Survey of Finland, Special Paper, 53, 35–138, 2012.
- Sappin, A.-A., Constantin, M., Clark, T., and van Breemen, O.: Geochemistry, geochronology, and geodynamic setting of Ni–Cu ± PGE mineral prospects hosted by mafic and ultramafic intrusions in the Portneuf–Mauricie Domain, Grenville Province, QuebecGéologie Québec Contribution 8439-2008-2009-5. Geological Survey of Canada Contribution 20080511, Canadian Journal of Earth Sciences, 46, 331–353, https://doi.org/10.1139/e09-022, 2009.
- Sappin, A.-A., Constantin, M., and Clark, T.: Origin of magmatic sulfides in a Proterozoic island arc an example from the Portneuf–Mauricie Domain, Grenville Province, Canada, Mineralium Deposita, 46, 211–237, https://doi.org/10.1007/s00126-010-0321-8, 2011.
- Saumur, B. and Cruden, A.: Ingress of magmatic Ni-Cu sulphide liquid into surrounding brittle rocks: Physical & structural controls, Ore Geology Reviews, 90, 439–445, 2017.
- Savard, D., Barnes, S. J., and Meisel, T.: Comparison between nickel-sulfur fire assay Te co-precipitation and isotope dilution with high-pressure asher acid digestion for the determination of platinum-group elements, rhenium and gold, Geostandards and Geoanalytical Research, 34, 281–291, 2010.
- Scheiber, T., Viola, G., Bingen, B., Peters, M., and Solli, A.: Multiple reactivation and strain localization along a Proterozoic orogen-scale deformation zone: the Kongsberg-Telemark boundary in southern Norway revisited, Precambrian Research, 265, 78–103, 2015.
- Scheiber, T., Viola, G., Ganerød, M., and Bingen, B.: 40Ar/39Ar constraints on the tectonic evolution of the central part of the Mesoproterozoic Sveconorwegian orogen, Journal of Structural Geology, 166, 104777, https://doi.org/10.1016/j.jsg.2022.104777, 2023.
- Sciuba, M., Beaudoin, G., Grzela, D., and Makvandi, S.: Trace element composition of scheelite in orogenic gold deposits, Mineralium Deposita, 55, 1149–1172, 2020.
- Slagstad, T., Marker, M., Roberts, N. M., Saalmann, K., Kirkland, C. L., Kulakov, E., Ganerød, M., Røhr, T. S., Møkkelgjerd, S. H., and Granseth, A.: The Sveconorwegian orogeny–Reamalgamation of the fragmented southwestern margin of Fennoscandia, Precambrian Research, 350, 105877, https://doi.org/10.1016/j.precamres.2020.105877, 2020.
- Slagstad, T., Henderson, I. H., Roberts, N. M., Kulakov, E. V., Ganerød, M., Kirkland, C. L., Dalslåen, B., Creaser, R. A., and Coint, N.: Anorthosite formation and emplacement coupled with differential tectonic exhumation of ultrahigh-temperature rocks in a Sveconorwegian continental back-arc setting, Precambrian research, 376, 106695, https://doi.org/10.1016/j.precamres.2022.106695, 2022.
- Slagstad, T., Skår, Ø., Bjerkan, G., Coint, N., Granseth, A., Kirkland, C. L., Kulakov, E., Mansur, E., Orvik, A. A., Petersson, A., and Roberts, N. M. W.: Subduction and loss of continental crust during the Mesoproterozoic Sveconorwegian Orogeny, Precambrian Research, 409, 107454, https://doi.org/10.1016/j.precamres.2024.107454, 2024.

- Sláma, J., Košler, J., Condon, D. J., Crowley, J. L., Gerdes, A., Hanchar, J. M., Horstwood, M. S., Morris, G. A., Nasdala, L., and Norberg, N.: Plešovice zircon a new natural reference material for U–Pb and Hf isotopic microanalysis, Chemical geology, 249, 1–35, 2008.
- Sobolev, A. V., Hofmann, A. W., Sobolev, S. V., and Nikogosian, I. K.: An olivine-free mantle source of Hawaiian shield basalts, Nature, 434, 590–597, 2005.
- Song, X., Wang, Y., and Chen, L.: Magmatic Ni-Cu-(PGE) deposits in magma plumbing systems: Features, formation and exploration, Geoscience Frontiers, 2, 375–384, https://doi.org/10.1016/j.gsf.2011.05.005, 2011.
- Spandler, C. J., Eggins, S. M., Arculus, R. J., and Mavrogenes, J. A.: Using melt inclusions to determine parent-magma compositions of layered intrusions: Application to the Greenhills Complex (New Zealand), a platinum group minerals—bearing, island-arc intrusion, Geology, 28, 991–994, https://doi.org/10.1130/0091-7613(2000)28<991:Umitdp>2.0.Co;2, 2000.
- Steadman, J. A., Large, R. R., Olin, P. H., Danyushevsky, L. V., Meffre, S., Huston, D., Fabris, A., Lisitsin, V., and Wells, T.: Pyrite trace element behavior in magmatic-hydrothermal environments: An LA-ICPMS imaging study, Ore Geology Reviews, 128, 103878, https://doi.org/10.1016/j.oregeorev.2020.103878, 2021.
- Stephens, M. B. and Wahlgren, C.-H.: Chapter 17 Accretionary orogens reworked in an overriding plate setting during protracted continent-continent collision, Sveconorwegian orogen, southwestern Sweden, Geological Society, London, Memoirs, 50, 435–448, 2020.
- Stephens, M. B., Wahlgren, C.-H., Weijermars, R., and Cruden, A. R.: Left-lateral transpressive deformation and its tectonic implications, Sveconorwegian orogen, Baltic Shield, southwestern Sweden, Precambrian Research, 79, 261–279, 1996.
- Torgersen, E., Gabrielsen, R. H., Ganerød, M., van der Lelij, R., Schönenberger, J., Nystuen, J. P., and Brask, S.: Repeated brittle reactivations of a pre-existing plastic shear zone: combined K–Ar and 40Ar–39Ar geochronology of the long-lived (> 700 Ma) Himdalen–Ørje Deformation Zone, SE Norway, Geological Magazine, 159, 2110–2131, 2022.
- Ulmius, J., Andersson, J., and Möller, C.: Hallandian 1.45 Ga high-temperature metamorphism in Baltica: P–T evolution and SIMS U–Pb zircon ages of aluminous gneisses, SW Sweden, Precambrian Research, 265, 10–39, 2015.
- Vermeesch, P.: IsoplotR: A free and open toolbox for geochronology, Geoscience Frontiers, 9, 1479–1493, 2018.
- Viola, G., Henderson, I., Bingen, B., and Hendriks, B.: The Grenvillian–Sveconorwegian orogeny in Fennoscandia: back-thrusting and extensional shearing along the "Mylonite Zone", Precambrian Research, 189, 368–388, 2011.
- Viola, G., Bingen, B., and Solli, A.: Berggrunnskart, Kongsberg litotektoniske enhet, Kongsberg-Modum-Hønefoss M 1:100000, Norwegian Geological Survey (NGU), https://www.ngu.no/publikasjon/berggrunnskart-kongsberg-litotektoniske-enhet-kongsberg (last access: 31 October 2025), 2016.
- Wahlgren, C.-H., Cruden, A. R., and Stephens, M. B.: Kinematics of a major fan-like structure in the eastern part of the Sveconorwegian orogen, Baltic Shield, south-central Sweden, Precambrian Research, 70, 67–91, 1994.

Wiedenbeck, M., Alle, P., Corfu, F., Griffin, W. L., Meier, M., Oberli, F. v., Quadt, A. v., Roddick, J., and Spiegel, W.: Three natural zircon standards for U-Th-Pb, Lu-Hf, trace element and REE analyses, Geostandards newsletter, 19, 1–23, 1995.

Wilson, A. H.: A Chill Sequence to the Bushveld Complex: Insight into the First Stage of Emplacement and Implications for the Parental Magmas, Journal of Petrology, 53, 1123–1168, https://doi.org/10.1093/petrology/egs011, 2012.